INT. REVIEWS IN PHYSICAL CHEMISTRY, 2004
VOL. 23, NO. 1, 79–108

Taylor & Francis
Taylor & Francis Group

Photofragment spectroscopy of covalently bound transition metal complexes: a window into C–H and C–C bond activation by transition metal ions

RICARDO B. METZ*

Department of Chemistry, University of Massachusetts, Amherst, MA 01003, USA

Transition metal cations M^+ and metal oxide cations MO^+ can activate C–H and C–C bonds in hydrocarbons. In this review, we discuss our studies of the electronic spectroscopy and dissociation dynamics of the intermediates, reactants and products of these reactions using photofragment spectroscopy. Results are presented on the spectroscopy of the intermediates of methane activation by FeO^+, as well as on the spectroscopy of FeO^+, NiO^+ and PtO^+. Resonance enhanced photodissociation allows us to measure the electronic spectroscopy of FeO^+ below the dissociation limit with rotational resolution. Complementary time-dependent B3LYP calculations of excited electronic states of FeO^+ and NiO^+ are in surprisingly good agreement with experiment. Dissociation onsets give upper limits to bond strengths for $FeCH_2^+$, $CoCH_2^+$, $NiCH_2^+$, $TaCH_2^+$ and $AuCH_2^+$. These results are compared to thermodynamic measurements, and the extent to which rotational energy contributes to dissociation is investigated. The spectroscopy of the π-bonded complexes $Pt(C_2H_4)^+$ and $Au(C_2H_4)^+$ is discussed, along with studies of larger systems. Planned studies of the vibrational spectroscopy of covalently bound ions are also discussed.

Contents

* E-mail: rbmetz@chemistry.umass.edu

International Reviews in Physical Chemistry ISSN 0144–235X print/ISSN 1366–591X online
http://www.tandf.co.uk/journals
DOI: 10.1080/01442350310001654065

1. Introduction

Transition metals are ubiquitous in chemistry, forming the basis for most catalysts, industrial and biological. Even isolated transition metal ions (M^+) in the gas phase have an extremely rich chemistry, activating C–H and C–C bonds in hydrocarbons [1–4]. In many cases, the transition metal oxides MO^+ are even more reactive, able to perform difficult oxidations such as the conversion of methane to methanol [5, 6]. Reactions of MO^+ have been proposed as models for methane activation in a wide range of systems, from iron-doped zeolites [7] to the enzyme-soluble methane monooxygenase [8], because they exhibit the desired chemistry and can be studied under well-defined conditions, free of complications from solvent and ligands.

The schematic potential energy surface for the reaction of Ta^+ with methane (figure 1) illustrates several general features. The reaction has entrance channel ($Ta^+\cdots(CH_4)$) and exit channel ($H_2\cdots TaCH_2^+$) complexes that are more stable than the reactants and products, respectively. This is a general feature of the potential for ion–molecule reactions caused by the electrostatic attraction between the reactants. (The entrance channel complex may not be stable, as is probably the case for $Pt^+\cdots(CH_4)$, where insertion of Pt^+ into the C–H bond is facile.) In addition, the potential energy surface has covalently bound intermediates that are also local minima—in fact, the global minimum on the $Ta^+ + CH_4$ potential corresponds to $[H–Ta–CH_3]^+$. These intermediates and complexes have a profound effect on the dynamics and products of the reaction [9].

The thread connecting our studies is the use of spectroscopy to illuminate the mechanism of C–H and C–C bond activation by transition metal-containing ions. In our studies, ion–molecule reactions are used to synthesize the intermediates of C–H and C–C bond activating reactions of M^+ and MO^+. The intermediates are subsequently cooled and we use photofragment spectroscopy to study their electronic spectroscopy. We also study the electronic spectroscopy of the molecular reactants and products of these reactions. Our studies complement full-collision reaction studies by directly probing the potential energy surface for the reaction and, in some cases, initiating the reaction from an intermediate with well-defined energy, orientation and angular momentum in a half-collision study [10, 11].

Photofragment spectroscopy, in which absorption of photons is monitored by photodissociation, has been widely used to study the electronic [10, 12, 13] and vibrational [14, 15] spectroscopy of metal-containing ions. Most studies of transition

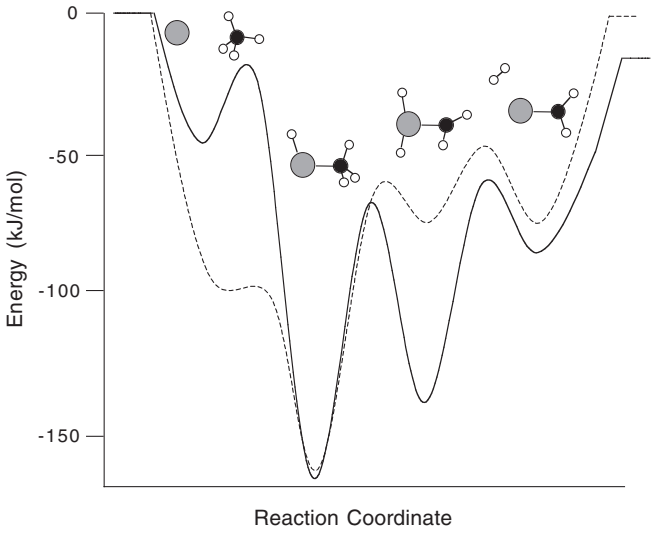

Figure 1. Schematic potential energy surfaces for the reactions $M^+ + CH_4 \rightarrow MCH_2^+ + H_2$ for $M^+ = Ta^+$ (solid line) and Pt^+ (dashed line). Structures of stable intermediates are also shown. In each case, only the lowest energy spin state is shown. The Ta^+ surface is based on calculations by Sändig and Koch [61]; the Pt^+ surface is based on experiments [64] and calculations [64, 110, 111] by several groups and on our calculations.

metal-containing systems have focused on electrostatically bound complexes, often as models for ion solvation. A characteristic feature of our work is the emphasis on studying covalently bound molecules (e.g. MCH_2^+) and intermediates (e.g. $[HO–Fe–CH_3]^+$). Photofragment spectroscopy not only allows us to study the electronic spectroscopy of these systems but also often gives information on bond strengths, as well as dissociation dynamics (fragmentation pathways and, in certain cases, kinetic energy release (KER)). Details of our experimental configuration and ion synthesis and also how we obtain thermodynamic and dynamical information are discussed below, followed by examples of systems we have studied. These include several ions involved in methane activation by M^+ and MO^+. Finally, the spectroscopy of larger ions that involve π bonding and C–C bond activation is covered, followed by planned extensions of these studies to measure the vibrational spectra of intermediates.

2. Experimental approach

The experiments described in this article were carried out by laser photofragment spectroscopy. In this technique, mass-selected ions are irradiated, typically using a laser. Ions that absorb light can photodissociate, producing fragment ions that are mass analysed and detected. Our photofragment studies are carried out in the dual time-of-flight mass spectrometer shown schematically in figure 2.

2.1. *Ion synthesis*

Ions are produced in a standard laser ablation source [16, 17]. The frequency-doubled output of a pulsed Nd:YAG laser (**A** in figure 2) operating at 20 Hz

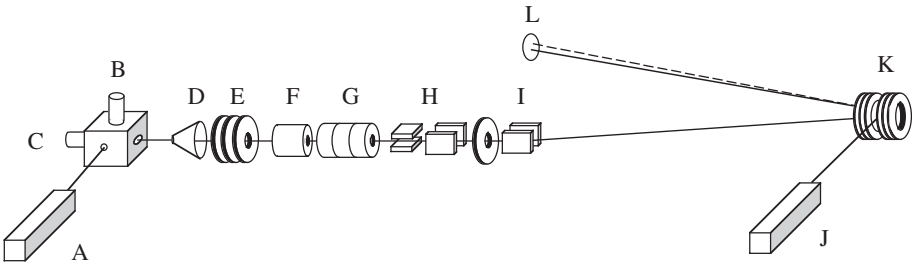

Figure 2. Time-of-flight photofragment spectrometer. See text for details.

repetition rate is loosely focused onto a rotating and translating metal rod (**B**). Transition metal ions M^+ are produced by ablation and react with an appropriate precursor that is entrained in a pulse of gas introduced through a piezoelectric pulsed valve (**C**) [18]. Metal–ligand complexes M^+L, where the ligand is a stable molecule (e.g. $M(C_2H_4)^+$), are produced using 0.3–5% ligand seeded in an inert carrier such as helium or argon at a backing pressure of 1–5 atm. However, in most of the ions we study the metal is covalently bound to a radical (e.g. MCH_2^+, MO^+). These ions are synthesized via ion–molecule reactions: MCH_2^+ is produced by reaction of M^+ with ethylene oxide (M = Fe, Co, Ni, Au). Cyclopropane and methane are suitable precursors for the more reactive third-row metals, while reaction of M^+ with nitrous oxide gives MO^+ [19].

Our choice of synthetic precursors is guided by the extensive literature on ion–molecule reactions, typically carried out under single-collision conditions in ion cyclotron resonance (ICR) spectrometers [1, 3]. Although conditions in our ablation source are very different from those in an ICR spectrometer, we generally observe the same products (although, of course, the ablation source also produces cluster ions). This was especially important in our study of intermediates of the $FeO^+ + CH_4$ reaction [20]. All of the intermediates have the stoichiometry $[Fe, C, O, H_4]^+$ and thus cannot be separated in our mass spectrometer, so it was critical to find precursors that selectively form each intermediate. Our choice was based on the extensive study of Schröder *et al.*, who produced several of the intermediates by reacting Fe^+ with a variety of neutral molecules in an ICR spectrometer [21]. They identified the resulting ions based on fragments produced after collision-induced dissociation (CID). Again, we were generally able to produce the desired intermediates using the same reaction. For example, the $[H_2C{=}Fe{-}OH_2]^+$ intermediate is made by the reaction of Fe^+ with acetic acid or, with less efficiency and specificity, *n*-propanol. Reaction of Fe^+ with methanol efficiently produces $[HO{-}Fe{-}CH_3]^+$; acetic acid and *n*-propanol also give modest yields of this isomer. In each case, we characterized the ion formed through its dissociation pathways and photodissociation spectrum [20].

Although ablation of the metal rod results in a plasma, we observe only small yields of ions that are the result of endothermic reactions. Thus, for example, yield of FeO^+ with CO_2 as a precursor is only 1% of that with N_2O. This can make synthesis of a desired ion awkward. The reaction of M^+ with ethylene oxide to form MCH_2^+ is exothermic and efficient for iron and cobalt, but is $\sim 17\,kJ\,mol^{-1}$ endothermic for nickel. As a result, our $NiCH_2^+$ yield is an order of magnitude smaller than that of

$FeCH_2^+$ and $CoCH_2^+$ [22]. Guided ion beam experiments show that, although the reaction

$$Ni^+ + N_2O \rightarrow NiO^+ + N_2 \quad (1)$$

is exothermic, it is spin forbidden and very inefficient [23]. We also find this to be the case in the ablation source, as we produce copious amounts of $Ni(N_2O)_n^+$ [24] and very little NiO^+.

Once formed, ions are cooled to reduce spectral congestion and minimize hot bands. Following ablation, ions travel through a tube of diameter 2.5 mm and length 2–10 mm, and supersonically expand into the source vacuum chamber. After 10 cm, the beam is skimmed (**D**) and ions pass into the differential pumping chamber. We have measured [25] a rotational temperature of 8 K for FeO^+, although the supersonic expansion is not at equilibrium, so the rotational state distribution has a small component at a higher temperature, which is not unusual for this type of source [26]. Using a rotational temperature to characterize an ion source can be misleading, as the reactions used to form the ions of interest can be fairly exothermic, producing vibrationally and even electronically excited ions. These degrees of freedom are more difficult to cool than rotations. Figure 3 shows the effect of vibrational cooling on the photodissociation spectrum of $Au(C_2H_4)^+$. Using helium in the expansion results in poor vibrational cooling. The broad peaks in the spectrum are probably due to overlapping vibrational sequence bands. Adding 5% CF_4 to the mixture greatly improves vibrational cooling, giving considerably sharper peaks.

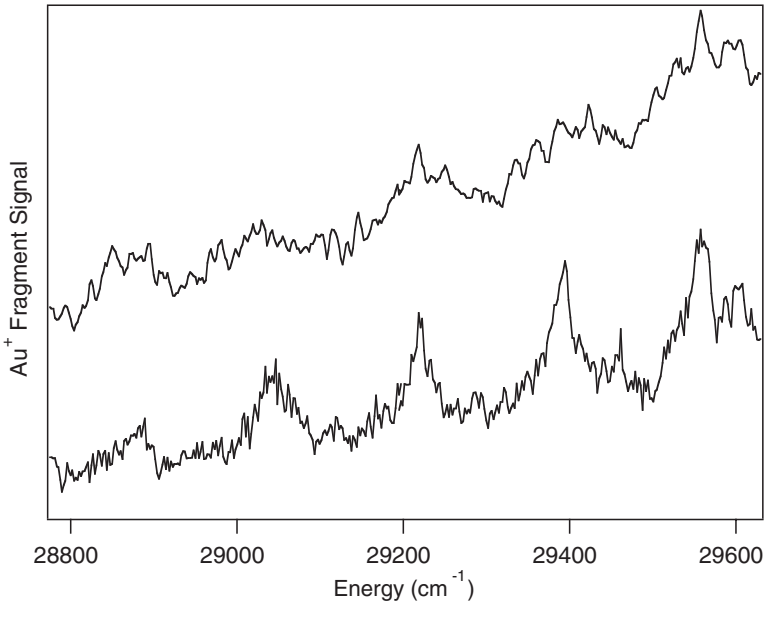

Figure 3. A portion of the photodissociation spectrum of $Au(C_2H_4)^+$ obtained by monitoring the Au^+ fragment. *Top*: Ions produced using 0.3% C_2H_4 seeded in helium. *Bottom*: Ions produced using 0.3% C_2H_4 and 5% CF_4 in helium. Adding CF_4 improves vibrational cooling, leading to a sharper photodissociation spectrum. The peaks spaced by $\sim 170\,cm^{-1}$ are due to a vibrational progression in the Au^+-ethylene stretch.

CF_4 is used because it has several low-frequency vibrations and is fairly unreactive. Transitions from vibrationally excited molecules can provide useful information, provided they can be identified and analysed. Hot FeO^+ (produced using 3% N_2O in helium) has a $(v'=1) \leftarrow (v''=1)$ sequence band that disappears when 15% N_2 is added to the carrier gas [25]. This sequence band allows us to measure the ground state vibrational frequency $v_0'' = 838 \pm 4\,cm^{-1}$. The ions we study tend to have many low-lying electronic states, often with different spin than the ground state, so it is not unusual to produce ions in metastable electronic states. Their presence can lead to errors in determining bond strengths. The dissociation onset of internally cold ions gives an upper limit to the bond strength. For many ions, the dissociation cross-section drops slowly, not suddenly, as one approaches the onset, and excited (especially electronically excited) ions can lead to a long-wavelength tail in the photodissociation spectrum. The photodissociation of $CoCH_2^+$ to $Co^+ + CH_2$ provides an example of this effect. Ions produced using a carrier gas that contains 5% O_2 show a fairly sharp onset at 361 nm; ions produced without O_2 show no sharp onset, and have extensive tailing to longer wavelength. Oxygen is especially good at cooling electronically excited molecules. Internally excited ions were also observed in the pioneering ICR photodissociation studies of Hettich and Freiser, who used collisions with argon to cool the ions, successfully in some cases (as with $CoCH_2^+$) [19]. In other cases this cooling was ineffective, leading to misassigned onsets and incorrect bond strengths (as with FeO^+) [27]. Transitions from metastable ions can give useful information on low-lying excited electronic states, which can be very difficult to obtain by other means. For example, in PtO^+ we have observed and analysed a transition from the metastable $^4\Delta_{7/2}$ state (the ground state is $^4\Sigma_{3/2}$) [28].

2.2. *Photofragment spectroscopy*

After the skimmer, ions are extracted along the beam axis using a pulsed electric field, then accelerated to 1800 V kinetic energy (**E**). This is a coaxial implementation of the popular orthogonal Wiley–McLaren time-of-flight mass spectrometer [29]. It is convenient to have the source and flight tube grounded, so, after acceleration, the ions must be re-referenced to ground potential [30]. This is accomplished by maintaining the re-referencing tube (**F**) at -1800 V as the ion cloud enters, then pulsing it to ground prior to the ions' exit using a potential switch [31]. An Einzel lens (**G**) and deflectors (**H**) guide the ions through an aperture into the detector chamber. A final deflector (**I**) allows the ion beam to traverse the 5° angle through the reflectron and to the detector. When the deflector is off, $<0.1\%$ of the incident ions reach the detector. Applying a pulsed voltage to the deflector allows only ions within a few mass units of the ion of interest to reach the detector, forming an effective mass gate. This is essential because, without the mass gate, peaks from lighter ions, particularly the large M^+ peak, affect the baseline for the rest of the mass spectrum. The mass gate passes ions lying within $\pm 2\%$ of the desired mass and, as ions are spatially compressed in the reflectron, we can simultaneously photodissociate ions with slightly different masses, such as $^{194}PtO^+$, $^{195}PtO^+$ and $^{196}PtO^+$. The range of the mass gate is a disadvantage if, for example, we wish to study dissociation of $[H–Pt–CH_3]^+$. Ablation of Pt^+ in CH_4/He also produces $PtCH_2^+$ and our current mass gate cannot separate these ions, so $PtCH_2^+$ parent signal interferes with the much smaller signal from photodissociation products of $[H–Pt–CH_3]^+$. In order to circumvent this problem, we have implemented a wire mesh mass gate with greatly improved resolution [32].

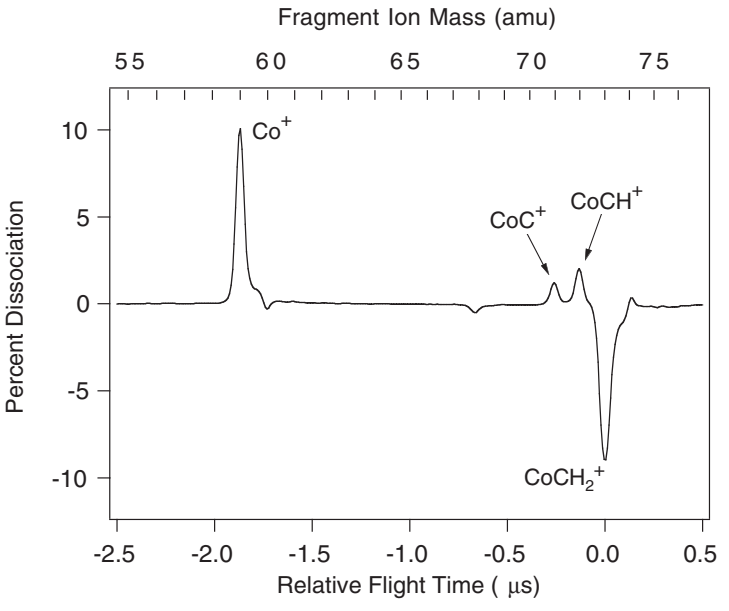

Figure 4. Difference mass spectrum of $CoCH_2^+$ at 320 nm. At this wavelength, dissociation occurs by three channels: loss of H, H_2 or CH_2.

Ions are photodissociated using the unfocused output of a pulsed, tunable dye laser pumped by an injection-seeded Nd:YAG (**J**). With mixing and doubling crystals, this laser system is tunable from 220 to >900 nm with $<0.08\,cm^{-1}$ line-width. The laser irradiates the mass-selected ion at the turning point [33] of the reflectron (**K**) [34, 35] and the masses of charged dissociation fragments (dashed line in figure 2) are determined by their subsequent flight times to a 40-mm diameter dual microchannel plate detector (**L**). The resulting signal is amplified, collected on a digital oscilloscope or a gated integrator and averaged using a LabView-based program. Subtracting mass spectra collected with the dissociation laser blocked from those when it is unblocked produces a *difference mass spectrum*. As shown in figure 4, this allows immediate identification of the dissociation channels active at a given wavelength, along with their relative importance. Mass resolution is $M/\Delta M \approx 200$ for fragment ions, although the large parent ion signal can make it difficult to detect H atom loss from heavier ions such as $AuCH_2^+$.

In some cases, the difference mass spectrum is also sensitive to KER and the dissociation rate. If the dissociation imparts significant kinetic energy to the fragments, their peaks in the difference mass spectrum will be broadened. We have used this to measure KER in the photodissociation of several dications to form two singly charged ions, where the total KER is 80–170 kJ mol^{-1} [36–38]. We have not yet observed significant tailing in photofragments of singly charged ions. There are several reasons for this. First, the long-range attraction between the fragments and the large number of available product quantum states both favour low KER. Second, the ions we have studied to date dissociate via loss of a light neutral, which leads to poor kinematics for the heavy, metal-containing ion that we detect. Photodissociation of ions with few product states can result in significant KER, as is observed for Mg_2^+, where Ding *et al.* have thoroughly analysed the KER and

photodissociation anisotropy [39]. If the ion is photoexcited and then travels some distance through the reflectron before it dissociates, its flight time will lie between those of the parent ion and prompt-dissociating fragments. The fragment peak in the difference mass spectrum will then exhibit an exponential tail whose time constant depends on the dissociation rate. In our apparatus, tailing should be observed for dissociation lifetimes in the range ~ 50 ns to ~ 3 μs. The upper limit is because ions that leave the reflectron prior to dissociating have the same flight time as the parent ions. We have not observed tailing for any singly charged, metal-containing ions, indicating photodissociation lifetimes below 50 ns. From the width of peaks in the photodissociation spectrum, the small ions we study typically dissociate in less than a picosecond. Larger ions do show tailing, for example ethylbenzene$^+$ near 450 nm [40], Fe_3-coronene$^+$ at 532 nm [41] and $Co^{2+}(CH_3OH)_4$ at 570 nm [38].

Monitoring the yield of a particular fragment ion as a function of laser wavelength and normalizing to parent ion signal and laser fluence yields the *photodissociation spectrum*. This is the absorption spectrum of those ions that photodissociate to produce the fragment being monitored. The photodissociation spectrum is obtained by monitoring fragment and parent ion signal with gated integrators or, if the fragment ion signal is very small, measuring the area under the fragment peak in the difference mass spectrum using numerical integration. Measurements of absolute photodissociation cross-sections are estimated to be accurate to within a factor of two, due to laser beam non-uniformity and uncertainty in laser beam overlap with the ion cloud. The uncertainty in relative cross-sections as a function of wavelength is much smaller, typically 10%.

The ions we study typically have several unpaired electrons and consequently have many excited electronic states. This high density of states, along with peak broadening due to photoinduced reactions, fast internal conversion and rapid dissociation, can lead to broad, featureless photodissociation spectra. Broad spectra can still contain valuable thermodynamic information, as one-photon dissociation of internally cold ions requires the photon energy to exceed the strength of the bond being broken. Photodissociation onsets thus give upper limits to the true thermodynamic bond strength [27, 42, 43]. The high density of electronic states in transition metal-containing ions means that they are likely to absorb widely in the visible and near UV. As a result of this broad absorption and strong coupling between states near the dissociation limit, these ions often photodissociate at the thermodynamic threshold, and the photodissociation onsets give very precise bond strengths [22, 44, 45]. In a few ions, the photodissociation spectrum exhibits vibrational structure that completely converges to a diabatic dissociation limit, allowing an even more precise determination of the bond strengths. This is the case for VAr^+ and $CoAr^+$, whose bond strengths have been measured with $< 0.1\ \mathrm{kJ\,mol^{-1}}$ precision [46–48]. Photodissociation studies thus complement collisional methods [43] (endothermic reactions or CID in guided ion beams), which are a much more general means to obtain bond strengths, as they do not rely on specific absorption properties of the molecule. An excellent review by Ervin [42] gives a detailed comparison of the methods used to measure ion thermochemistry.

Many of the ions we study have photodissociation spectra with resolved vibrational progressions and, in some cases, residual rotational structure. Analysis of the spectra gives detailed information on the excited state potential energy surface, coupling between electronic states, and the geometry of the ion. Our apparatus was designed, and is best suited to, measuring *structured* photodissociation spectra.

Much of the early work on photodissociation of organometallic ions and also several recent studies have been carried out with a very different apparatus: an ICR spectrometer using a lamp–monochromator combination as a light source [27]. In general, ICR spectrometers are better suited to measuring low-resolution spectra of larger, more complex ions. In an ICR spectrometer, consecutive ion–molecule reactions can be used to synthesize a complex ion in a controlled fashion. The extremely high mass resolution is useful when dealing with heavy ions, and the long observation times reduce the kinetic shifts due to slow dissociation of large ions near threshold. Advantages of our time-of-flight instrument include a higher repetition rate and the ability to produce rotationally cold ions. In each case, rapidly tunable light sources with modest resolution are useful for preliminary studies, and for some ions we have measured survey spectra using a 355 nm pumped broadband OPO tunable from 430–700 nm.

3. Methane activation

While reactions of first- and second-row transition metal cations with methane are endothermic [1], most third-row transition metal ions spontaneously dehydrogenate methane [49, 50]:

$$M^+ + CH_4 \rightarrow MCH_2^+ + H_2. \tag{2}$$

This reaction is exothermic if $D_0^\circ(M^+–CH_2) \geq 464\,\mathrm{kJ\,mol^{-1}}$. Often, sequential reactions exhibiting Fischer–Tropsch-type methylene coupling are observed:

$$MCH_2^+ + (n-1)CH_4 \rightarrow MC_nH_{2n}^+ + (n-1)H_2. \tag{3}$$

Irikura and Beauchamp report oligomerizations forming compounds as large as $WC_8H_{16}^+$ [49]. These reactions are the gas-phase analogue of the surface chemistry in which incorporation of hydrocarbons into the M–CH_2 bond of methylene chemisorbed onto metal surfaces is a crucial chain growth step in the Fischer–Tropsch process [51]. Studies of isolated, gas-phase MCH_2^+ offer the opportunity to understand the intrinsic properties of these systems.

3.1. *Using photodissociation to measure M^+–CH_2 bond strengths: $FeCH_2^+$, $CoCH_2^+$ and $NiCH_2^+$*

Because Fischer–Tropsch catalysis overwhelmingly uses Group VIII metals, we first studied the metallocarbenes MCH_2^+, where M = Fe, Co and Ni. In 1986, Hettich and Freiser studied the photodissociation of $FeCH_2^+$ and $CoCH_2^+$ in an ICR cell using a lamp–monochromator combination with low (10 nm) resolution [19]. We observe the same dissociation pathways, but improved resolution and ion cooling lead to more resolved spectra and more accurate photodissociation onsets. As shown in figure 4, several channels compete in the photodissociation of MCH_2^+. Loss of CH_2 by simple bond fission predominates over most of the spectrum; rearrangement and loss of H_2 is an interesting, but generally minor, pathway. Figure 5 shows the photodissociation spectrum of $FeCH_2^+$. The photodissociation onset is at 350 nm, which gives an Fe–CH_2^+ bond strength of $\leq 342 \pm 2\,\mathrm{kJ\,mol^{-1}}$ [22]. This is in complete agreement with $D_0^\circ(Fe^+–CH_2) = 341 \pm 4\,\mathrm{kJ\,mol^{-1}}$ measured by Schultz and Armentrout using a guided ion beam spectrometer [4, 52]. Unlike many transition metal dimers [44] M_2^+, the metallocarbenes we have studied do not exhibit sharp

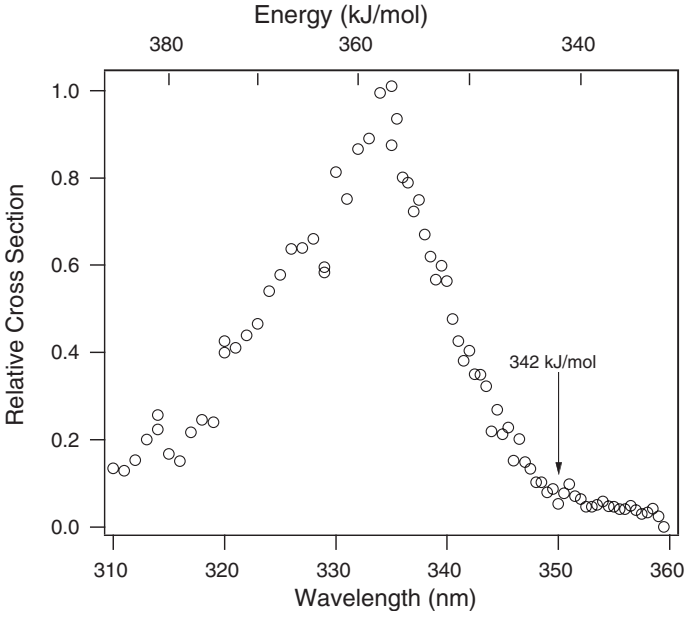

Figure 5. Photodissociation spectrum of $FeCH_2^+ + h\nu \rightarrow Fe^+ + CH_2$. A relative cross-section of 1 corresponds to $\sigma \approx 4 \times 10^{-18}\,cm^2$.

Table 1. Comparison of spectroscopic thresholds and thermodynamic bond strengths for MCH_2^+.

	Spectroscopic threshold ($kJ\,mol^{-1}$)	Thermodynamic bond strength ($kJ\,mol^{-1}$)
$FeCH_2^+$	342 ± 2 [22]	341 ± 4 [60]
$CoCH_2^+$	331 ± 2 [22]	318 ± 5 [60]
$NiCH_2^+$	295 ± 5 [22]	306 ± 4 [60]
$NbCH_2^+$	456 ± 29 [62]	428 ± 9 [153]
$RhCH_2^+$	372 ± 21 [62]	356 ± 8 [60]
$LaCH_2^+$	444 ± 21 [62]	401 ± 7 [60]
$TaCH_2^+$	480 ± 5	> 464 [49]
$AuCH_2^+$	372 ± 3 [55]	> 385; < 398 [57–59]

Thermodynamic values for $TaCH_2^+$ and $AuCH_2^+$ are based on observed reactions—see text for details.

photodissociation onsets. This is probably because the density of electronic states just above the dissociation limit is much lower for the metallocarbenes [22]. Table 1 compares the spectroscopic upper limits to M^+–CH_2 bond strengths measured in our group and by Hettich and Freiser using photodissociation to thermodynamic values obtained in guided ion beam experiments by Armentrout and co-workers, or from ion–molecule reactions. The results are in good agreement, with the spectroscopic values generally very close to the thermodynamic value.

The photodissociation spectrum of $FeCH_2^+$ (figure 5) shows no sharp structure, and this is true of all of the metallocarbenes we have studied. The sharpest features

are three 200 cm^{-1} wide peaks observed well above threshold in $CoCH_2^+$ [22]. This is in contrast to many other ions we have studied that have features with 1–20 cm^{-1} linewidths. The lack of structure could be due either to direct dissociation following photoexcitation to a repulsive excited state or to excitation to a bound excited state, followed by very rapid internal conversion and subsequent dissociation. A means to distinguish between these two possibilities suggested itself when we obtained the photodissociation spectrum of $[H_2C{=}Fe{-}OH_2]^+$. This is an intermediate of the $FeO^+ + CH_4$ reaction that leads to the minor, but thermodynamically favoured, $FeCH_2^+ + H_2O$ products. In this ion, B3LYP calculations show that the H_2O ligand has little effect on the $FeCH_2^+$ chromophore, so photodissociation of $[H_2C{=}Fe{-}OH_2]^+$ allows us to study the (slightly perturbed) spectroscopy of $FeCH_2^+$ below the Fe^+–CH_2 dissociation limit. From 400 to 750 nm, we observe transitions to at least three excited electronic states, each with $\sim$300 cm^{-1} wide peaks in an extended vibrational progression [20]. Having located the excited electronic states, we used resonance enhanced photodissociation (REPD) to study them in bare $FeCH_2^+$. In this technique, one photon promotes ions to an excited electronic state that lies below the dissociation limit. These excited ions then absorb a second photon and dissociate. In this study (and in our later work on FeO^+) we performed one-colour REPD, using two photons from the same laser pulse. Low signal levels precluded two-colour (two-laser) REPD experiments, which can give information on excited state dynamics. REPD can give spectra with laser-limit linewidth, as in our study of FeO^+ discussed below. However, resonance-enhanced photodissociation of $FeCH_2^+$ near 600 nm yields a spectrum very similar to that of $[H_2C{=}Fe{-}OH_2]^+$, with $\sim$300 cm^{-1} wide features, so even low-lying electronic states of $FeCH_2^+$ show rapid internal conversion.

3.2. *Rotational energy contributes to photodissociation: variable temperature photodissociation of $AuCH_2^+$*

The experimental observation that several third-row transition metal ions activate methane under thermal conditions has prompted theoreticians to examine these systems. The large number of electrons, along with significant relativistic effects, make these ions very challenging to theory. In fact, relativistic effects must be included to obtain accurate M^+–CH_2 bond strengths for the third-row transition metals [50, 53, 54]. $AuCH_2^+$ is closed shell and thus is one of the simplest of the third-row MCH_2^+ to treat theoretically, making it a benchmark system. We observe two pathways:

$$AuCH_2^+ + h\nu \nearrow \quad Au^+(^1S_0) + CH_2(X, ^3B_1) \tag{4}$$

$$AuCH_2^+ + h\nu \searrow \quad AuC^+\left(X, ^1\Sigma\right) + H_2\left(X, ^1\Sigma\right) \tag{5}$$

Surprisingly, the branching ratio is essentially constant at 1 : 1.4 (Au^+ : AuC^+) over the region studied, although production of Au^+ is spin forbidden [55, 56]. Unlike many of the other MCH_2^+, the Au^+–CH_2 bond strength has not been measured via endothermic reactions in a guided ion beam. $AuCH_2^+$ is produced by the reaction of Au^+ with CH_3Cl and CH_3Br, but not with CH_3I under thermal conditions in an ICR spectrometer [57, 58]. $AuCH_2^+$ competes with adduct formation in the reaction of state-selected Au^+ ($^1S_0$) with CH_3Br at 150 K in a drift cell [59]. These results imply that $D_0^o(Au^+{-}CH_2)$ lies between 385 and 398 kJ mol^{-1}.

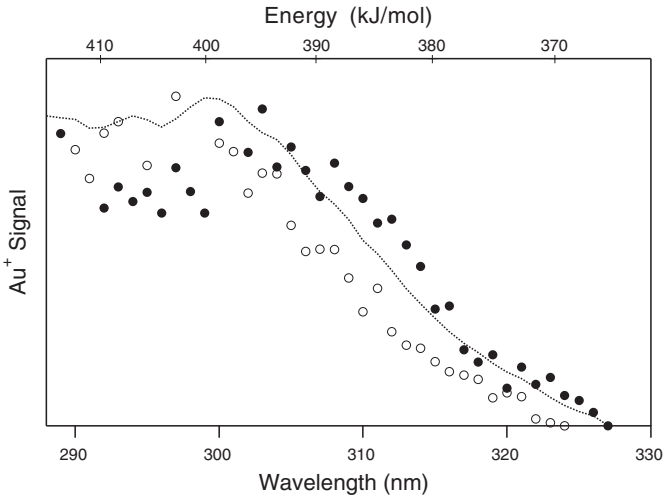

Figure 6. Photodissociation spectrum of $AuCH_2^+ + h\nu \rightarrow Au^+ + CH_2$. Open circles: jet-cooled ions; closed circles: rotationally thermalized (298 K) $AuCH_2^+$ ions. The dotted line is obtained by convoluting the photodissociation spectrum of jet-cooled ions with the rotational energy distribution of $AuCH_2^+$ at 298 K.

We have measured [55] the photodissociation spectrum of $AuCH_2^+$ and have used this system to address a fundamental question: to what extent does parent rotational energy contribute to the energy required to break a bond? Figure 6 shows the photodissociation spectrum of $AuCH_2^+$ obtained by monitoring the Au^+ fragment. Photodissociation of jet-cooled ions formed in the laser ablation source is shown with open circles. In order to study the effect of parent rotational energy on the photodissociation spectrum, the source was modified to allow ions to be trapped and rotationally thermalized after formation and supersonic expansion. We installed an rf quadrupole ion trap after the ablation source. Ions formed in the source collect in the trap, where they undergo ~ 30 collisions with helium buffer gas and are rotationally thermalized to 298 K. The vibrational population should not be affected, as the molecule has no low-frequency vibrations, and vibrational energy transfer with helium is inefficient [55]. The photodissociation spectrum of the thermalized ions shifts to lower energy, as shown in figure 6. Convoluting the photodissociation spectrum of internally cold ions with a calculated 298 K rotational distribution (dotted line) shows that the shift is due to parent rotational energy contributing to dissociation. An analogous effect is seen in bimolecular ion–molecule reactions, where energy in *all* reactant degrees of freedom has to be included to obtain accurate thermochemistry [60].

3.3. *Other third-row MCH_2^+*

Several third-row transition metal cations react exothermically with methane to produce MCH_2^+. Of these, WCH_2^+, $TaCH_2^+$ and $PtCH_2^+$ are particularly interesting because of their subsequent reactivity with methane [49]. We have carried out preliminary studies of $TaCH_2^+$ and $PtCH_2^+$. The photodissociation spectrum of $TaCH_2^+$ is unstructured and shows an onset at 249 nm, giving $D_0^\circ(Ta^+–CH_2) \leq 480 \pm 5\,kJ\,mol^{-1}$. The only other experimental determination of this value is based on the

efficient reaction [49] of Ta^+ with CH_4, which implies $D_0^o(Ta^+–CH_2) \geq 464\,kJ\,mol^{-1}$. Calculations predict $480 \pm 20\,kJ\,mol^{-1}$ [50] and $\leq 500\,kJ\,mol^{-1}$ [61]. Hettich and Freiser have studied photodissociation of $LaCH_2^+$, along with $NbCH_2^+$ and $RhCH_2^+$ at low resolution, measuring thresholds for loss of H, H_2 and CH_2 [62]. Simon *et al.* have photodissociated WCH_2^+ formed in the reaction of W^+ with CH_4 in an ICR spectrometer [63]. They observe loss of H atom starting at 2.5 ± 0.1 eV and calculate that the metallocarbene and $HWCH^+$ isomers are nearly isoenergetic. For many of the third-row MCH_2^+, loss of H atom occurs at lower energy than CH_2 loss. Unfortunately, for third-row metals we cannot detect the MCH^+ product in the difference mass spectrum of MCH_2^+ as it is hidden by the wings of the much larger parent peak. Future experiments on MCD_2^+ should avoid this problem.

Reaction of Pt^+ with methane has been studied extensively because of its interesting reactivity and the broad range of platinum-based catalysts in industry. Zhang *et al.* have studied the reactions of Pt^+ and CID of $PtCH_2^+$ in a guided ion beam spectrometer, determining $D_0^o(Pt^+–CH_2) = 463 \pm 3\,kJ\,mol^{-1}$ [64]. Reaction of Pt^+ with methane in the presence of a buffer gas, or of $Pt^+(Ar)_n$ with methane [65], produces the $[H–Pt–CH_3]^+$ intermediate, which is the minimum on the $Pt^+ + CH_4$ potential (see figure 1). CID shows that this intermediate lies $171 \pm 8\,kJ\,mol^{-1}$ below $Pt^+ + CH_4$ [64]. We plan to continue our studies of $PtCH_2^+$ and study the $[H–Pt–CH_3]^+$ intermediate and their deuterated analogues.

As noted earlier, methane activation by M^+ occurs via intermediates with a metal–methyl bond. A few of the simpler MCH_3^+ ions have been studied by photodissociation. Freiser and co-workers looked at $FeCH_3^+$ and $CoCH_3^+$; they each have a strong, broad absorption band in the near-UV that leads exclusively to loss of CH_3 [27]. We have studied $FeCH_3^+$ from 320 to 410 nm. As a result of our higher resolution, we observe partially resolved vibrational structure to long wavelength. As shown in figure 1, the reactions of some M^+ with methane proceed via a discrete $M^+(CH_4)$ entrance channel complex. We plan to study the spectroscopy of complexes of Ta^+ and FeO^+ (see below) with CH_4. Brucat and co-workers have obtained the photodissociation spectrum of $V(CH_4)^+$. It is complex, with extensive progressions in the metal–ligand stretch and rock [66].

4. Methane–methanol conversion

Direct oxidation of methane to an easily transportable liquid such as methanol has attracted great experimental and theoretical interest because of its importance as an industrial process and as the simplest alkane oxidation [67–69]. No direct, efficient methane–methanol conversion scheme has yet been developed [67], but significant advances have been made using iron-based catalysts. Wang and Otsuka have studied the direct oxidation of methane to methanol using an $FePO_4$ catalyst, with N_2O and H_2/O_2 as the oxidizing agents [70, 71]. Although high catalytic selectivity is obtained for methanol, the reaction yield is low. Other approaches that have achieved modest success include direct oxidation by nitrous oxide in a plasma [72], oxidation of methane to a methyl ester using a platinum catalyst [73], and direct methane–methanol conversion using an iron-doped zeolite [74]. In biological systems, methane–methanol conversion occurs efficiently and is catalysed by the enzyme methane monooxygenase (MMO). The active site of the enzyme contains non-heme iron centres [75–77].

In 1990, Schröder and Schwarz reported that gas-phase FeO^+ directly and efficiently converts methane to methanol under thermal conditions [78]. Reactions of gas-phase transition metal oxides with methane are thus a simple model system for the direct conversion of methane to methanol that is sufficiently small to be amenable to detailed experimental and theoretical study. As a result, these reactions have been studied extensively by experiment [5, 21, 78–80] and theory [21, 81–86]. We have used photofragment spectroscopy to study FeO^+ [25, 87], NiO^+ and PtO^+ [28] (all of which convert methane to methanol), as well as several intermediates of the $FeO^+ + CH_4$ reaction [20, 88].

4.1. *General considerations and reaction studies*

The partial oxidation of methane to methanol

$$\tfrac{1}{2}O_2 + CH_4 \rightarrow CH_3OH \tag{6}$$

is exothermic by $126\,kJ\,mol^{-1}$ [89]. In its simplest form, the catalytic conversion of methane to methanol by M^+/MO^+ can be written as

$$M^+ + \tfrac{1}{2}O_2 \rightarrow MO^+; \tag{7}$$

$$MO^+ + CH_4 \rightarrow M^+ + CH_3OH. \tag{8}$$

Reaction (7) is exothermic if $D_0^o(M^+–O) > 249\,kJ\,mol^{-1}$, and reaction (8) is exothermic if $D_0^o(M^+–O) < 375\,kJ\,mol^{-1}$. Figure 7 shows M^+–O bond strengths for the transition metals. Values are from Armentrout and Kickel [60] for the first-row metals and from Schröder *et al.* [6] for the second- and third-row metals, except for platinum [90]. Metals with values of $D_o(M^+–O)$ within the limits imposed by reactions (7) and (8) (dashed lines in figure 7) are in bold. The early transition metals bind so strongly to oxygen that reaction of MO^+ with methane is

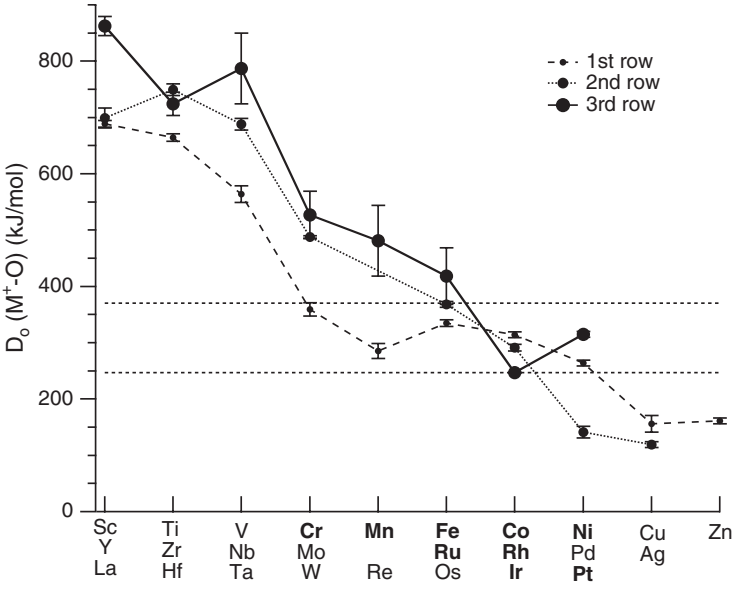

Figure 7. M^+–O bond strengths. The region between the dashed lines indicates values of D_0 for which reactions (7) and (8) are exothermic. The corresponding metals are in bold.

Table 2. Reactions of MO^+ with methane at thermal energies. Values are from [5], except for: (*a*) 1990 ICR study [78]; (*b*) 1997 ICR study [79]; (*c*) 1997 SIFT study [79].

MO^+	% Efficiency	$M^+ + CH_3OH$	$MOH^+ + CH_3$	$MCH_2^+ + H_2O$
MnO^+	40	< 1	100	–
FeO^{+a}	20	41	57	2
FeO^{+b}	9	39	61	trace
FeO^{+c}	7	18	82	–
CoO^+	0.5	100	–	–
NiO^+	20	100	–	–
PtO^+	100	25	–	75

endothermic, while some of the late transition metals bind oxygen so weakly that reaction (7) is endothermic, although MO^+ may react efficiently with methane. The reactions of many of these metal oxide cations have been investigated experimentally, and the results, where reaction is observed, are summarized in Table 2. These studies are single-collision, thermal reactions in an ICR cell [5, 78], complemented by multiple-collision thermal flow tube (SIFT) studies [79]. Many of these results have been discussed in reviews by Schröder, Schwarz and co-workers [1, 5, 6, 91] and by Metz [88].

4.2. *Reaction mechanism*

Bond activation by transition metals is a complex process, as it often involves making and breaking several bonds and occurs on multiple, coupled potential energy surfaces. Detailed understanding of the mechanism thus requires synergy between experiment and theory. This involves calculating not only the ground potential energy surface but also excited potential energy surfaces, often of different multiplicity, and the coupling between these surfaces. The quality of the calculations can then be evaluated by comparison with detailed experiments. Studies of small model systems that retain the essential chemistry are a key step in this process, as they are the systems for which we have the most detailed experimental results and the highest level calculations, allowing us to assess the reliability of competing theoretical methods. These methods can then be used to predict mechanisms for more complex reactions for which we have limited experimental data, or to help to develop improved catalysts.

An excellent example of the synergy between experiment and theory is the detailed mechanism that has been developed for the conversion of methane to methanol by MO^+. This mechanism includes two key concepts: concerted reaction involving the critical $[HO–M–CH_3]^+$ insertion intermediate and, for most metals, two-state reactivity. Figure 8 shows a schematic potential energy surface for the conversion of methane to methanol by FeO^+. This is an extension of calculations at the B3LYP/6-311G(d,p) level by Yoshizawa *et al.* on methane activation by FeO^+ [82, 83, 86] and the other first-row metals [84, 85]. Schröder *et al.* [21] and Fiedler *et al.* [81] have also carried out calculations on methane–methanol conversion by FeO^+ and the late first-row transition metals, respectively. In figure 8 the solid line indicates the sextet (high-spin) reaction path, the quartet path is dotted, and the minor pathway leading to $FeCH_2^+ + H_2O$ is in long dashes. The relative energies of reactants and products are based on established thermodynamics [89]. The energies of intermediates are based on our calculations [20, 92] at the B3LYP/6-311+G(d,p)

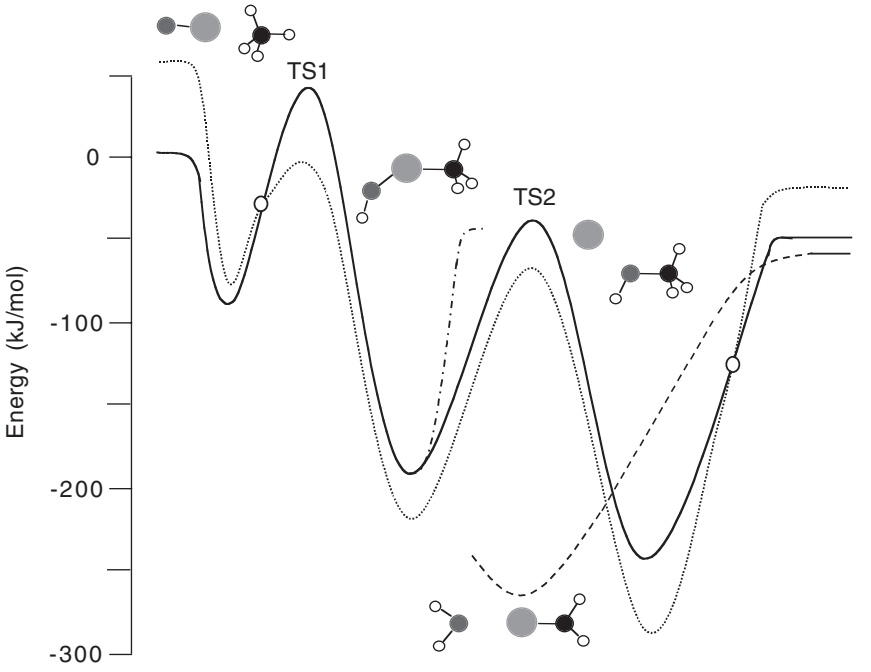

Figure 8. Schematic potential energy surface for the $FeO^+ + CH_4$ reaction and structures of stable intermediates. Solid line, sextet surface; short dash, quartet surface; long dash, $FeCH_2^+ + H_2O$ pathway; dot–dash, $FeOH^+ + CH_3$ pathway. Spin crossings are indicated by circles.

level, and the energies of transition states are relative to the previous intermediate, as calculated by Yoshizawa *et al*. [84].

The reaction proceeds as follows: electrostatic interaction between FeO^+ and methane produces the $[OFe\cdots CH_4]^+$ entrance channel complex. Depending on the level of theory, the Fe coordinates to either two (quartet state, and sextet state at B3LYP/6-311G(d,p)) or three (sextet state at B3LYP/6-311 + G(d,p)) hydrogens. In a classic case of back bonding, the iron removes electron density from the C–H σ bonding orbital and donates electrons to an Fe–C bonding, C–H anti-bonding orbital, weakening the C–H bond. At transition state TS1 the strong C–H bond in methane is being replaced by two bonds: a strong O–H bond and a fairly weak Fe–C bond. Although the reactants are high spin, at TS1 the low-spin state is significantly energetically favoured. TS1 leads to the key insertion intermediate $[HO–Fe–CH_3]^+$, which can dissociate to produce $FeOH^+ + CH_3$ or can undergo migration of a methyl group via TS2 to produce the iron/methanol exit channel complex $[Fe(CH_3OH)]^+$, which subsequently dissociates. Calculations performed by Schröder *et al*. [21] at the MP2/ECP-DZ level of theory suggest that the minor $FeCH_2^+ + H_2O$ product channel is derived from the dissociation of an aquo iron carbene intermediate $[H_2C{=}Fe–OH_2]^+$ that is separated from the insertion intermediate by a substantial barrier.

The potential energy surface shown in figure 8 allows us to make several predictions about the reaction. First, although both reactants and products are high spin, at thermal energies the reaction occurs through low-spin intermediates [83, 86].

In the figure, spin crossings are indicated schematically by circles. This 'two-state reactivity' has been extensively studied by Schröder, Shaik and co-workers, especially in the exothermic but very inefficient $FeO^+ + H_2 \rightarrow Fe^+ + H_2O$ reaction [93–96]. The *efficiency* of the reaction is determined by the energy of TS1 on the quartet surface, as well as by the lifetime of the $[OFe\cdots CH_4]^+$ entrance channel complex, which determines the likelihood of crossing to the quartet surface. The low efficiency of the $FeO^+ + H_2$ reaction is due to the short lifetime of the entrance channel complex. In general, the *selectivity* of the reaction between $M^+ + CH_3OH$ (methanol) and $MOH^+ + CH_3$ (methyl radical) products is determined primarily by the energy of TS2 relative to methyl radical products. Because MOH^+ is produced by simple bond fission of the insertion intermediate, it is entropically favoured over the methanol channel, which occurs through the tighter transition state TS2. Thus, if TS2 is at an energy close to or above the methyl products, the reaction will overwhelmingly produce $MOH^+ + CH_3$, as is observed for MnO^+. Similarly, in the iron system, where TS2 lies somewhat below the methyl radical products, the two pathways are competitive, but increased translational energy strongly favours the methyl radical pathway [79].

4.3. *Photodissociation spectroscopy of MO^+*

In contrast to the many experimental studies of *reactions* of MO^+, there have been few studies of their spectroscopy. Photoelectron spectroscopy of the neutral oxides is challenging because of the high temperatures required to produce a useful vapour pressure, but has been used by Dyke and co-workers to investigate VO^+, CrO^+, NbO^+ and TaO^+ with vibrational resolution [97–99]. Weisshaar and co-workers used a laser ablation source to produce a cold molecular beam and REMPI pulsed field ionization to obtain rotationally resolved photoelectron spectra of TiO and VO, measuring rotational constants of the corresponding ions [100, 101].

More recently, photodissociation has emerged as a powerful tool for studying these ions. Hettich *et al.* studied FeO^+ at low (~ 10 nm) resolution in an ICR spectrometer [27]. Our group has studied predissociation of FeO^+, NiO^+ and PtO^+ (discussed later). In these studies, the dissociation lifetime limits the resolution to 1–200 cm^{-1}, depending on the system. For higher resolution studies, resonance enhanced photodissociation is very promising, as the resolution is typically limited by the laser linewidth to $\sim 0.05\,cm^{-1}$. In this technique, a photon electronically excites molecules to a state below the dissociation limit; they then non-resonantly absorb a second photon and dissociate. Brucat and co-workers [26] demonstrated the power of this technique in their study of $^5\Phi_5$–$^5\Delta_4$ and $^5\Pi_3$–$^5\Delta_4$ transitions in CoO^+, and our group [87] has recently applied it to a $^6\Sigma$–$^6\Pi$ transition in FeO^+. In each case, detailed analysis of the rotationally resolved spectrum gives bond lengths and a wealth of rotational constants.

The electronic structure of MO^+ has been the subject of numerous theoretical studies. Most of these studies are covered in Harrison's excellent review article [102]. Detailed descriptions of bonding in the first-row transition metal MO^+ have been given by Carter and Goddard [103], Fiedler *et al.* [81], Bauschlicher and co-workers [104] and, recently, by Nakao *et al.* [105]. The reactions of FeO^+ and PtO^+ are especially interesting, and these ions have been studied in detail by Fiedler *et al.* [106] and Heinemann *et al.* [107].

4.3.1. *FeO^+ and NiO^+: TD-DFT calculations and dissociation dynamics*

Coordinatively unsaturated compounds containing transition metals have many low-lying excited electronic states. Recently, time-dependent density functional (TD-DFT) calculations have emerged as a surprisingly accurate, efficient way to characterize the excited states of these complex molecules. Following Borowski and Broclawik's study [108] of neutral VO and MoO, we have investigated FeO^+, NiO^+ and PtO^+ using TD-DFT, obtaining results in excellent agreement with experiment. Figure 9 shows potentials for the ground and some excited electronic states of NiO^+ (left) and FeO^+ (right). The excited electronic states were calculated by TD-DFT, so only states that can be reached by a spin-allowed, one-electron transition from the ground state are shown. The horizontal lines in figure 9 indicate the bond dissociation energy D_e (based on experimental D_o and corrected for zero-point energy) [3]. Both NiO^+ and FeO^+ have quasi-bound excited electronic states that lie near the dissociation limit and are good candidates for photodissociation studies. Because of the $\sim 2000\,cm^{-1}$ error in the calculated excitation energies (see below), it turns out that the lowest vibrational state of the $^6\Sigma$ excited state of FeO^+ lies above the dissociation limit. The figure does not show, nor have we calculated, the couplings between the excited states (and with other excited states of lower spin) that would lead to predissociation and spectral broadening.

To assess the reliability of these calculations we have also calculated [87] excited states of MnO and CrF, which are isoelectronic with FeO^+ and have been well characterized by spectroscopy. The large number of unpaired electrons and the

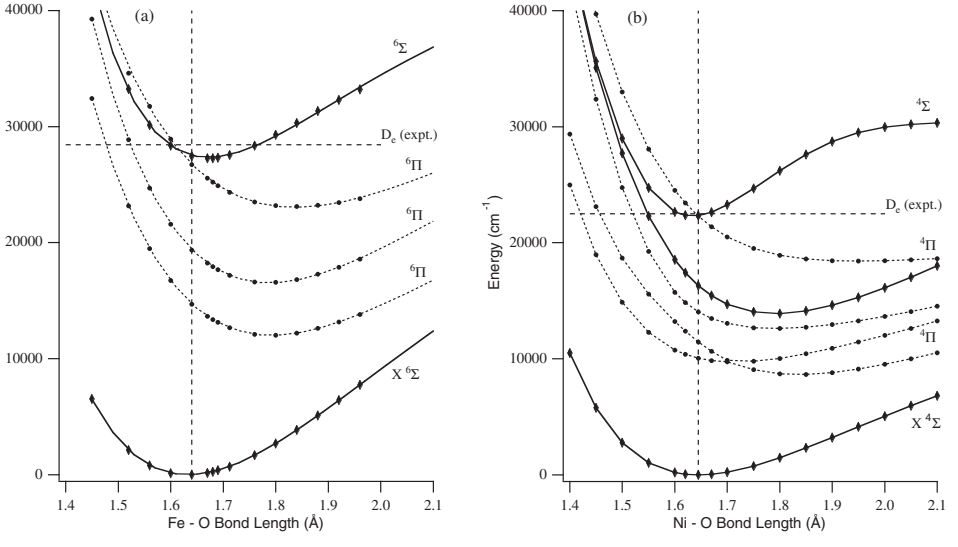

Figure 9. Potential energy curves for (*a*) NiO^+ and (*b*) FeO^+. In each case, the ground electronic state and excited states accessible by allowed electronic transitions from the ground state are shown. Curves are calculated using B3LYP/TD-DFT with a 6-311 + G(d,p) basis set for NiO^+ and 6-311G(d,p) for FeO^+. Solid lines indicate Σ states; dashed lines are Π states. The vertical dashed line is at r_e for the ground state. The horizontal dashed line is at the dissociation energy D_e, obtained by correcting experimental D_0 for vibrational zero-point energy.

presence of low-lying electronic states make the calculations especially challenging. Including FeO^+, the bond lengths, excitation energies and vibrational frequencies are calculated with a mean error of 0.03 Å, and 2000 and 50 cm^{-1}, respectively. The deviation in the calculated excitation energies is consistent with the 1500 cm^{-1} deviation obtained by Borowski and Broclawik [26] for VO and MoO. It is our experience that TD-DFT is an inexpensive, reliable tool in predicting low-lying excited electronic states of small transition metal-containing systems. The method is sufficiently simple and efficient that, for new ions, we routinely use TD-DFT calculations to select initial photodissociation wavelengths.

For NiO^+ we observe a broad, structureless band at 23 130 cm^{-1} (2.867 eV) (80 cm^{-1} FWHM) and unstructured dissociation to higher energy. This is likely to be the transition from the $^4\Sigma$ ground state to the $^4\Sigma$ excited state that lies just above the dissociation limit [60] of 22 200 ± 400 cm^{-1}. Tuning below the dissociation limit, we observe fairly efficient one-colour resonance enhanced (1 + 1) photodissociation, but the spectrum is structureless, suggesting that there is strong coupling between states.

The photodissociation spectrum of FeO^+ is much richer. Figure 10 shows the origin of the $^6\Sigma \leftarrow X\,^6\Sigma$ band, which lies just above the dissociation limit [60] of 28 000 ± 400 cm^{-1}. The asymmetry in the peak is due to unresolved rotational structure, which can be simulated to obtain rotational constants for the upper state, using the known (see below) constants for the lower state [25, 87]. The resolution is limited to 1.5 cm^{-1} by the 3.5 ps dissociation lifetime. The $v' = 1$ peak is observed 662 cm^{-1} higher in energy and is 40 cm^{-1} wide, dissociating in 140 fs. By running under conditions that minimize vibrational cooling, we observe the $1 \leftarrow 1$ transition at 28 473 cm^{-1}, which allows us to also measure the vibrational frequency in the ground electronic state $v_0'' = 838\ cm^{-1}$ [25].

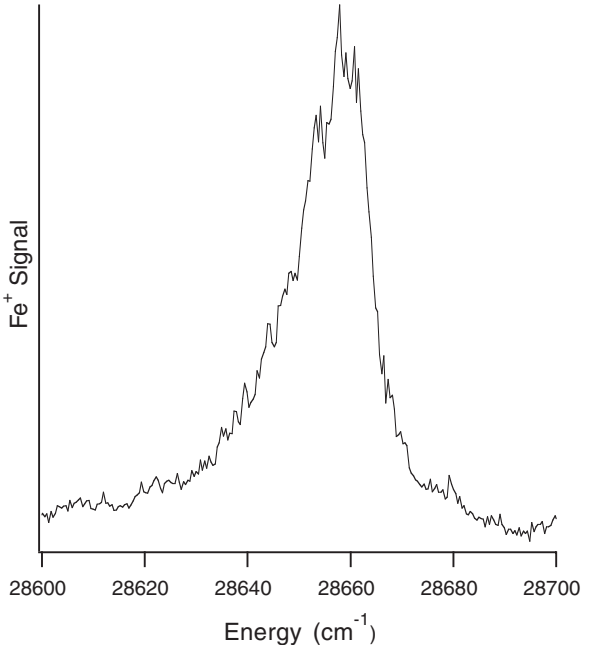

Figure 10. Photodissociation spectrum of FeO^+: the 0–0 band of the $^6\Sigma \leftarrow X\,^6\Sigma$ system.

4.3.2. *Spectroscopy of FeO^+ below the dissociation limit*

To overcome limitations on resolution imposed by the excited state lifetime we have carried out one-colour resonance enhanced $(1+1)$ photodissociation studies of FeO^+ [87]. Figure 11 shows the region of the spectrum with transitions from $v''=0$ of the $^6\Sigma$ ground state to $v'=8$ of the $^6\Pi_{7/2}$ excited state. The vibrational numbering is based on the shift observed for the minor $^{54}FeO^+$ isotopomer. The observed linewidth is $0.05\,cm^{-1}$, which is the linewidth of the laser. At this resolution, we can clearly resolve rotational structure. The $^6\Sigma$ ground state has six spin–spin sublevels and we observe transitions from four of them. We have assigned the transitions to $v'=8,9$ of the $^6\Pi_{7/2}$ excited state and have fit them to a detailed Hamiltonian to obtain rotational constants for the ground and $^6\Pi_{7/2}$ excited states. The rotational constant $B_o=0.5020\pm0.0004\,cm^{-1}$ for the ground state, giving $r_o=1.643\pm0.001$ Å. Other molecular parameters determined for the $^6\Sigma^+$ ground state are the spin–spin (second-order spin–orbit) coupling constant, $\lambda=-0.126\pm0.006\,cm^{-1}$, and the spin–rotational coupling constant, $\gamma=-0.033\pm0.002\,cm^{-1}$. The $^6\Pi$ state in this transition corresponds to the lowest of the $^6\Pi$ states shown in figure 9. Observation of transitions to high vibrational levels of the $^6\Pi$ state is consistent with the calculations, which predict that the low-lying $^6\Pi$ states have charge-transfer character, with much longer bond length than the $^6\Sigma$ ground state. These detailed experimental

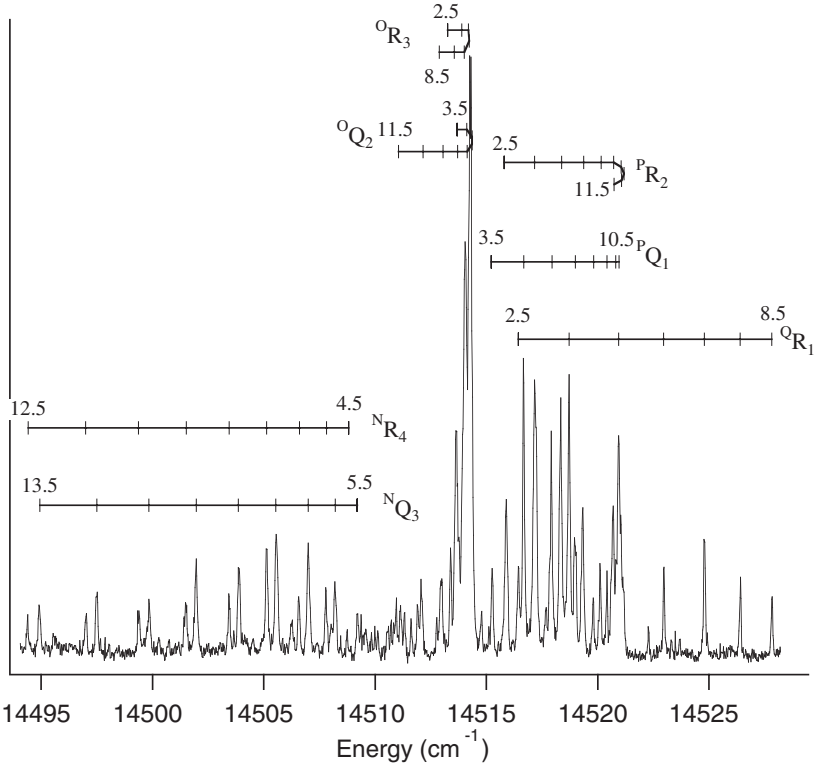

Figure 11. Resonance enhanced $(1+1)$ photodissociation spectrum and rotational assignments of the $v'=8\leftarrow v''=0$ band of the $^6\Pi_{7/2}\leftarrow{}^6\Sigma^+$ system of FeO^+. The subscripts indicate the spin component of the ground state (F_1 is $\Sigma=5/2$), while the superscripts indicate ΔN for the transition.

findings on FeO^+ and similar metal-containing systems provide a demanding test of theory. Measurements of the ground state bond length and the ground and excited state vibrational frequencies test calculations of the electronic potentials, while measurements of the spin–spin and spin–orbit splitting test calculations of the couplings between states.

4.3.3. *The complex spectrum of PtO^+*

PtO^+ reacts with methane at the collision rate, producing methanol with 25% selectivity [109]. This is an essential step in the catalytic conversion of methane to methanol by gas-phase Pt^+ [110]. The catalytic cycle begins with methane activation

$$Pt^+ + CH_4 \rightarrow PtCH_2^+ + H_2, \tag{9}$$

which was discussed in section 3. The metallocarbene then reacts with oxygen:

$$PtCH_2^+ + O_2 \begin{cases} \nearrow PtO^+ + H_2CO\ (30\%). & (10) \\ \searrow Pt^+ + [C, H_2, O_2]\ (70\%). & (11) \end{cases}$$

Methanol is generated and Pt^+ is recovered via

$$PtO^+ + CH_4 \rightarrow Pt^+ + CH_3OH. \tag{12}$$

These reactions have been studied in extensive ICR experiments by Schwarz and co-workers and theoretically by Siegbahn and co-workers [109–111]. We have studied the spectroscopy of PtO^+ and plan to also study the intermediates of reactions (9)–(12).

The photodissociation spectrum of PtO^+ (figure 12) is the most complex we have observed for a small molecule. There are over 100 vibrational peaks in the 5000 cm^{-1} range covered; many of the peaks are only $\sim 5\,cm^{-1}$ wide and contain partially resolved rotational structure. From the onset to photodissociation (shown by the arrow in figure 12) we obtain $D_0^o(Pt^+–O) \leq 305\,kJ\,mol^{-1}$; guided ion beam experiments by Zhang and Armentrout give $D_0^o(Pt^+–O) = 315 \pm 7\,kJ\,mol^{-1}$ [90]. Calculations on PtO^+ at the CAS–SCF level, including spin–orbit and relativistic core effects, predict a $^4\Sigma$ ground state. Spin–orbit effects in this molecule are large, leading to a large spin–spin (second-order spin–orbit) splitting in the ground state: the ground state is calculated to be $^4\Sigma_{3/2}$, with the $^4\Sigma_{1/2}$ lying 400 cm^{-1} higher [111]. Spin–orbit effects should lead to extensive perturbations in the excited states of PtO^+, as is observed in calculations on isoelectronic $PtCH_2^+$ [112]. We have identified [28] three vibrational progressions, shown in figure 12, based on the requirements that there are several peaks in the progression, all with similar rotational contours, reasonable intensities, and with a good fit to a Morse progression. Rotational simulations show that in each of these states the bond is 0.11–0.15 Å longer than in the ground state. All of the peaks that could be fit to a rotational contour are due to transitions from a $^4\Sigma_{3/2}$ state, confirming that this is the ground state. The only exception to this is the cluster of small peaks just to the left of the arrow in figure 12, and shown in more detail in figure 13. The intensity of this feature depends on source conditions, identifying it as a hot band. Rotational analysis identifies it as a $\Omega = 7/2 \leftarrow \Omega = 7/2$ transition, probably from the metastable $^4\Delta_{7/2}$ electronic state [28].

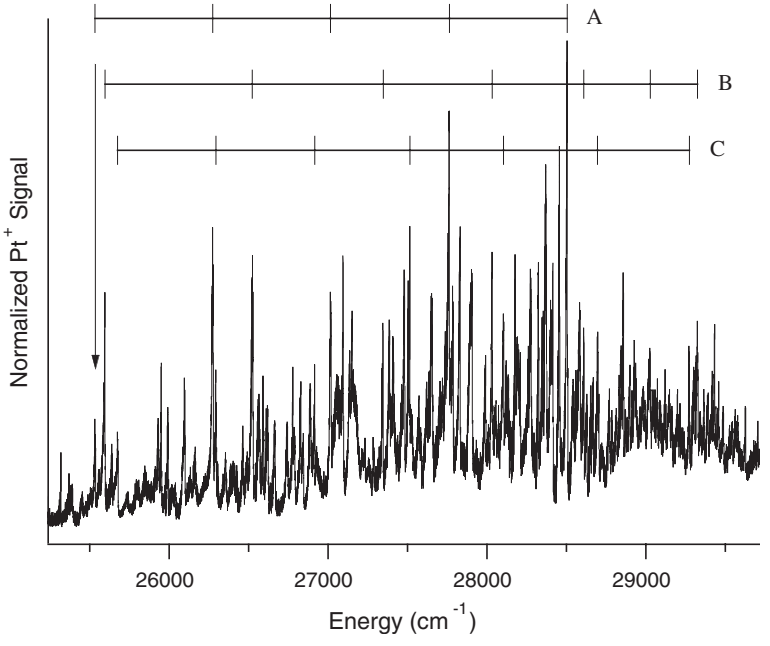

Figure 12. Photodissociation spectrum of PtO^+. The three excited state vibrational progressions labelled A, B and C are due to transitions to $^4\Pi_{-1/2}{}^4\Pi_{5/2}$ and $^4\Pi_{-1/2}$ states, respectively, from the $^4\Sigma_{3/2}$ ground state. The photodissociation onset of 25 520 cm^{-1} is indicated by the arrow. The small peaks to lower energy are due to a hot band.

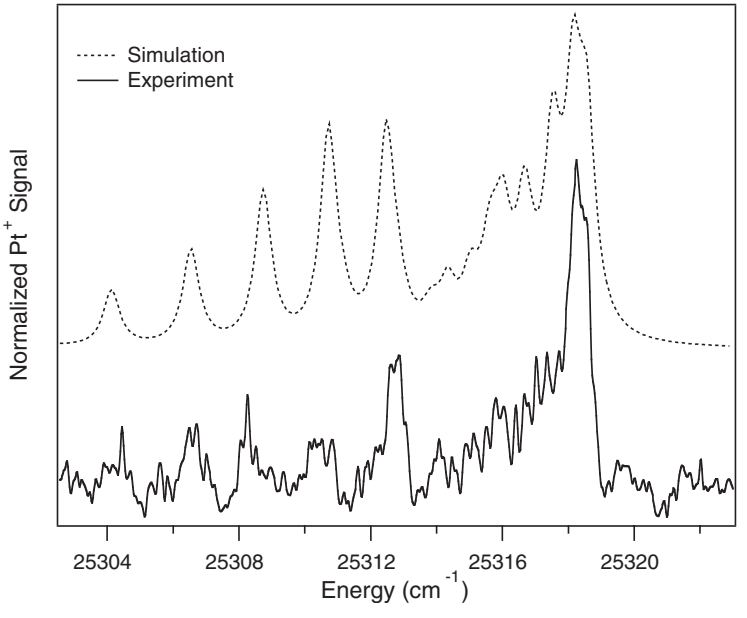

Figure 13. Photodissociation spectrum of a hot band of PtO^+. The rotational simulation (dashed line) indicates a $\Omega = 7/2 \leftarrow \Omega = 7/2$ transition, probably from the metastable $^4\Delta_{7/2}$ electronic state. Parameters are $B'' = 0.392\,cm^{-1}$, $B' = 0.285\,cm^{-1}$ and a 5 ps lifetime.

4.4. *Spectroscopy of intermediates of methane–methanol conversion by FeO^+*

The potential energy surface for the $FeO^+ + CH_4$ reaction features four distinct intermediates (figure 8). If these intermediates are formed and cooled, they should be stable in the absence of collisions and they can be studied. In an elegant series of experiments, Schröder *et al*. produced these intermediates by reacting Fe^+ with organic precursors in an ICR cell. The intermediates were characterized based on fragment ions produced by CID [21]. As discussed in section 2.1, we produce the $[HO–Fe–CH_3]^+$ and $[H_2O–Fe=CH_2]^+$ intermediates using specific ion–molecule reactions, cool them in a supersonic expansion, and measure their photodissociation spectra. Details on the technique, ion characterization and results on the $[H_2O–Fe=CH_2]^+$ intermediate are given elsewhere [20, 92]. The photodissociation spectra of $[HO–Fe–CH_3]^+$ and $[HO–Fe–CD_3]^+$ obtained by monitoring $FeOH^+$ are shown in figure 14. The spectrum is vibrationally resolved and the peaks show some tailing to lower energy due to unresolved rotational structure. Photodissociation of the insertion intermediate produces $Fe^+ + CH_3OH$ and $FeOH^+ + CH_3$ in a 44:56 ratio at each peak. Photodissociation away from a peak gives increased production of the non-reactive $FeOH^+$ channel (33:67 ratio). Thus, in this half-collision experiment, photoexcitation of the $[HO–Fe–CH_3]^+$ intermediate triggers the $FeO^+ + CH_4$ reaction, leading to the same products as are observed in the bimolecular reaction. As these intermediates are probably in the sextet state [20], the peaks are due to vibrations in an electronically excited sextet state of the intermediate. They have been assigned to an extended progression in the Fe–C stretch ($\nu_{11} = 478\,cm^{-1}$) and short progressions in the Fe–O stretch ($\nu_8 = 861\,cm^{-1}$) and O–Fe–C bend ($\nu_{14} = 132\,cm^{-1}$). This assignment is supported by isotope shifts in the spectrum of the partially deuterated species $[HO–Fe–CD_3]^+$ and extensive hybrid density functional theory (B3LYP) calculations [20]. The Franck–Condon simulation shown in the figure

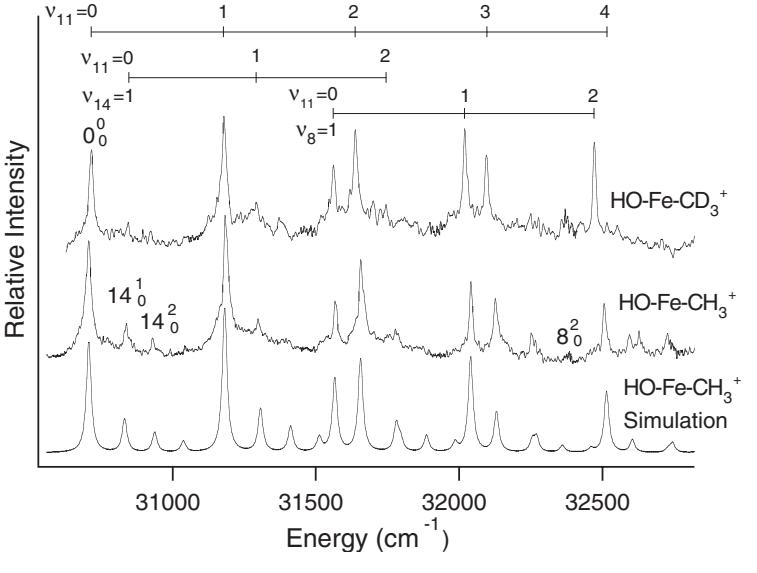

Figure 14. Photodissociation spectra of insertion intermediates of the $FeO^+ + CH_4$ reaction, with vibrational assignments. *Top*: $[HO–Fe–CD_3]^+$; *middle*: $[HO–Fe–CH_3]^+$; *bottom*: Franck–Condon simulation of the $[HO–Fe–CH_3]^+$ spectrum.

predicts that electronic excitation leads to a 0.13 Å change in the Fe–C bond length, a 0.05 Å change in the Fe–O bond length, and an O–Fe–C angle change of 4°.

5. Larger hydrocarbons

Consecutive reactions of several third-row transition metal cations M^+ with methane produce $M^+C_nH_{2n}$ (reaction (3)). These molecules are attractive candidates for further study, to elucidate their structure. Simon and co-workers have used a Xe arc lamp and monochromator to study photodissociation of $Ta^+(C_2H_4)$ formed by sequential reaction of Ta^+ with two methane molecules [113]. They calculate nine low-energy isomers, and conclude that the reaction produces the lowest energy $(H)_2Ta^+(C_2H_2)$ isomer based on the observed photolysis by loss of H_2 and C_2H_2. Au^+ and Pt^+ bind surprisingly strongly to C_2H_4 ($D_o(M^+–C_2H_4) = 288$ and 231 kJ mol^{-1}, respectively) [114]. Based on the strength of the $Au^+–C_2H_4$ bond and calculations, it has been suggested that $Au(C_2H_4)^+$ is best described as a metallocyclopropane rather than a metal–π complex [115, 116]. We have studied photodissociation of jet-cooled $Au(C_2H_4)^+$ and $Pt(C_2H_4)^+$ formed by reaction of M^+ with ethylene [117]. Photodissociation occurs by loss of C_2H_4 and, to a lesser extent, loss of H_2. A portion of the photodissociation spectrum of $Au(C_2H_4)^+$ is shown in figure 3. The photodissociation spectrum of $Pt(C_2H_4)^+$ (figure 15) shows two peaks, a small feature at 450 nm and a larger peak at 330 nm. Both peaks are broad, and scans show that, unlike $Au(C_2H_4)^+$, the photodissociation spectrum of $Pt(C_2H_4)^+$ lacks sharp structure. Freiser and co-workers have also studied the

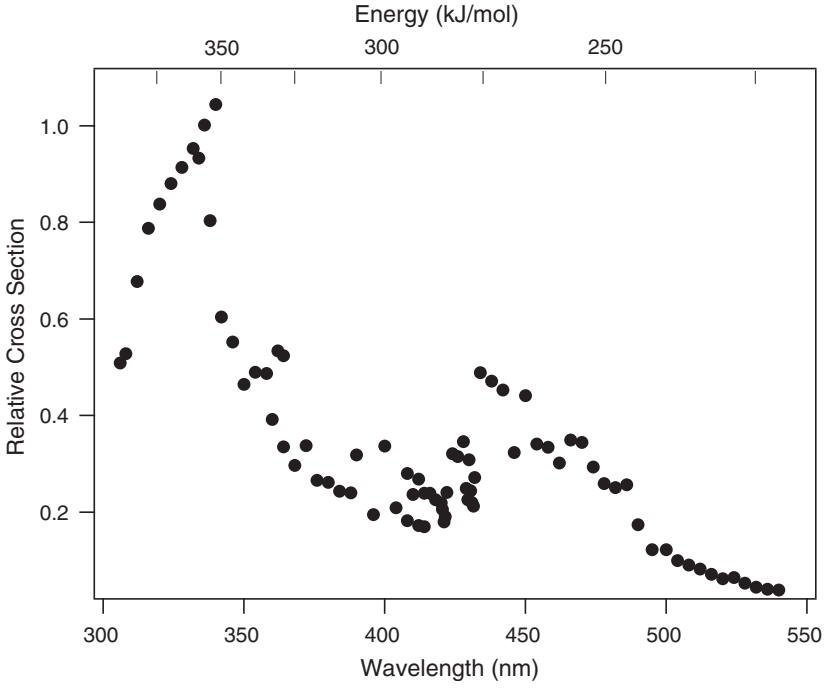

Figure 15. Photodissociation spectrum of $Pt(C_2H_4)^+$ obtained by monitoring the Pt^+ fragment. A relative cross-section of 1 corresponds to $\sigma \approx 6 \times 10^{-19}$ cm^2.

photodissociation of $Fe(C_2H_4)^+$ and $La(C_2H_4)^+$, which occur by ligand loss, at low resolution [118, 119]. Kleiber and co-workers have measured the photodissociation spectrum of jet-cooled $Zn(C_2H_4)^+$, observing several electronic bands, some of which are vibrationally and partially rotationally resolved [120]. At low energy dissociation is primarily by ligand loss, but charge transfer (to produce $C_2H_4^+$, $C_2H_2^+$ and $C_2H_3^+$) becomes increasingly important at higher energy. They observe a similarly rich spectroscopy and dynamics for $Zn(CH_4)^+$ and $Zn(CH_3OH)^+$ [121, 122].

The spectroscopy of several M^+ complexes with acetylene has been studied. Ranasinghe and Freiser measured photodissociation thresholds for ligand loss from $M^+(C_2H_2)$ (M = Sc, Y, La), obtaining $218 \pm 13\,kJ\,mol^{-1}$ for all three systems [123]. Ranatunga and Freiser photodissociated $Nb^+(C_2H_2)$ and $Zr^+(C_2H_2)$ using single lines from an Ar^+ laser, again obtaining dissociation thresholds [124]. Duncan and co-workers recently demonstrated the power of infrared spectroscopy to probe structure and intracluster reactions in transition metal complexes [15]. Spectra of $Ni(C_2H_2)_n^+$ ($n = 3$–6) in the C–H stretch region show that a second shell commences with $n = 5$. At this cluster size, new bands appear, indicating formation of π-bonded cyclobutadiene formed by an intracluster cyclization reaction [125].

Several first-row transition metal cations activate C–H and C–C bonds in propane and larger hydrocarbons under thermal conditions, producing H_2 and CH_4, respectively. This is surprising in light of the difficulty of activating C–H and, especially, C–C bonds in solution. Consequently, these reactions have been studied extensively [1]. For example, reactions of Co^+ and Ni^+ with propane have been studied by many experimental techniques, under single and multiple collision conditions, and as a function of collision energy [126–133]. We carried out preliminary photodissociation studies of $Fe(C_3H_6)^+$, observing production of Fe^+ with a large cross-section.

There have been several studies of the photodissociation of transition metal cation complexes with larger ligands. Hettich *et al*. generated four distinct isomers of $Ni(C_4H_8)^+$ and two isomers of $Fe(C_4H_6)^+$ using ion–molecule reactions and showed that they have different photodissociation spectra and dissociation pathways [27]. They also studied Co(1-pentene)$^+$ [134]. Complexes with aromatic molecules have been studied by several groups. Because of the low ionization potential of the ligand, charge transfer pathways (producing, for example, $C_6H_6^+$) are often observed. Photodissociation studies of M(benzene)$^+$ include Ag [135], Co [27], Cu [135], Fe [27, 135], La [119], Sc [136], Ta [137] and V [27, 137]. In addition, complexes of Ag^+ with acetone, toluene [135] and pyridine [138] have been studied, along with Cu^+-pyridine [138] and Ta^+-benzyne [137]. Nanayakkara and Freiser also studied photodissociation of complexes of Co^+ with pyrrole, furan and thiophene [139]. Several other iron-containing ions have been studied by Freiser and co-workers: $Fe(C_6H_4)^+$, $Fe(C_6H_5)^+$, $(H)Fe(C_5H_5)^+$, $Fe(C_7H_7)^+$ and $Fe(C_8H_{10})^+$ [140–142].

6. Future directions

Research in our group on the spectroscopy of ions involved in C–H and C–C bond activation is moving in two general directions. The systems we have studied to date are fairly small, and we plan to look at larger intermediates such as those involved in propane activation by Co^+ and Ni^+. On moving to larger systems, it becomes increasingly important to investigate complexes using complementary techniques, and even for small molecules, electronic spectroscopy of jet-cooled ions

gives little information on the vibrations of the ground electronic state. Hence we will pursue studies of the vibrational spectroscopy of ions in concert with our work on their electronic spectroscopy. Although infrared multiphoton dissociation (IRMPD) studies of transition metal-containing cations [143–146] were first carried out some two decades ago, they are hampered by the limited tunability of the CO_2 lasers used. The recent development of laboratory OPO/OPA systems tunable from 2000 to more than 4000 cm^{-1}, as well as synchrotron-based free-electron lasers tunable throughout the infrared, has revitalized this field [15, 147]. We shall soon use an OPO/OPA to study the vibrational spectroscopy of the ground electronic state of intermediates of methane activation by M^+ and MO^+. These studies seek to determine the structure and bonding of the intermediates and to elucidate the mechanism of ligand activation by the metal centre. We will also continue to explore stimulated Raman excitation to prepare vibrationally excited molecules [148, 149] in order to study skeletal vibrations, which lie outside the range of the OPO/OPA. Vibrationally excited molecules will be detected by monitoring the dissociation of molecules 'tagged' with a weakly bound spectator molecule [150, 151], or as a result of selective photodissociation of vibrationally excited molecules (vibrationally mediated photodissociation) [148, 152].

Acknowledgements

Financial support from the Camille and Henry Dreyfus Foundation (New Faculty Award) and the National Science Foundation under award numbers CHE-9875220 and CHE-0308439 is gratefully acknowledged. The studies outlined in this article are the work of many talented group members: graduate students Fernando Aguirre, Murat Citir, Kieron Faherty, John Husband, Kay Stringer and Chris Thompson and undergraduates Victoria Campbell, Peter Ferguson, Chris Laperle and Melanie McWilliams.

References

[1] K. Eller and H. Schwarz, Chem. Rev. **91**, 1121 (1991).
[2] J. C. Weisshaar, Acc. Chem. Res. **26**, 213 (1993).
[3] B. S. Freiser (editor), *Organometallic Ion Chemistry* (Kluwer Academic Publishers, Dordrecht, 1996).
[4] P. B. Armentrout, in *Organometallic Bonding and Reactivity: Fundamental Studies*, edited by J. M. Brown and P. Hofmann (Springer-Verlag, Berlin, 1999).
[5] D. Schröder and H. Schwarz, Angew. Chem., Int. Ed. Engl. **34**, 1973 (1995).
[6] D. Schröder, H. Schwarz, and S. Shaik, Struct. Bonding **97**, 91 (2000).
[7] K. Yoshizawa, Y. Shiota, T. Yumura, and T. Yamabe, J. Phys. Chem. B **104**, 734 (2000).
[8] K. Yoshizawa, J. Biol. Inorg. Chem. **3**, 318 (1998).
[9] R. J. Green and S. L. Anderson, Int. Rev. Phys. Chem. **20**, 165 (2001).
[10] P. D. Kleiber and J. Chen, Int. Rev. Phys. Chem. **17**, 1 (1998).
[11] J. M. Mestdagh, B. Soep, M. A. Gaveau, and J. P. Visticot, Int. Rev. Phys. Chem. **22**, 285 (2003).
[12] M. A. Duncan, Int. J. Mass Spectrom. **200**, 545 (2000).
[13] R. C. Dunbar, Int. J. Mass Spectrom. **200**, 571 (2000).
[14] J. M. Lisy, Int. Rev. Phys. Chem. **16**, 267 (1997).
[15] M. A. Duncan, Int. Rev. Phys. Chem. **22**, 407 (2003).
[16] T. G. Dietz, M. A. Duncan, D. E. Powers, and R. E. Smalley, J. Chem. Phys. **74**, 6511 (1981).

[17] P. J. Brucat, L.-S. Zheng, C. L. Pettiette, S. Yang, and R. E. Smalley, J. Chem. Phys. **84**, 3078 (1986).
[18] D. Proch and T. Trickl, Rev. Sci. Instrum. **60**, 713 (1989).
[19] R. L. Hettich and B. S. Freiser, J. Am. Chem. Soc. **108**, 2537 (1986).
[20] F. Aguirre, J. Husband, C. J. Thompson, K. L. Stringer, and R. B. Metz, J. Chem. Phys. **116**, 4071 (2002).
[21] D. Schröder, A. Fiedler, J. Hrusák, and H. Schwarz, J. Am. Chem. Soc. **114**, 1215 (1992).
[22] J. Husband, F. Aguirre, C. J. Thompson, C. M. Laperle, and R. B. Metz, J. Phys. Chem. A **104**, 2020 (2000).
[23] P. B. Armentrout, L. F. Halle, and J. L. Beauchamp, J. Chem. Phys. **76**, 2449 (1982).
[24] D. Bellert, T. Buthelezi, V. Lewis, K. Dezfulian, and P. J. Brucat, Chem. Phys. Lett. **240**, 495 (1995).
[25] J. Husband, F. Aguirre, P. Ferguson, and R. B. Metz, J. Chem. Phys. **111**, 1433 (1999).
[26] A. Kamariotis, T. Hayes, D. Bellert, and P. J. Brucat, Chem. Phys. Lett. **316**, 60 (2000).
[27] R. L. Hettich, T. C. Jackson, E. M. Stanko, and B. S. Freiser, J. Am. Chem. Soc. **108**, 5086 (1986).
[28] C. J. Thompson, K. L. Stringer, M. McWilliams, and R. B. Metz, Chem. Phys. Lett. **376**, 588 (2003).
[29] W. C. Wiley and I. H. McLaren, Rev. Sci. Instrum. **26**, 1150 (1955).
[30] L. A. Posey, M. J. DeLuca, and M. A. Johnson, Chem. Phys. Lett. **131**, 170 (1986).
[31] R. E. Continetti, D. R. Cyr, and D. M. Neumark, Rev. Sci. Instrum. **63**, 1840 (1992).
[32] J. R. Kimmel, F. Engelke, and R. N. Zare, Rev. Sci. Instrum. **72**, 4354 (2001).
[33] D. S. Cornett, M. Peschke, K. Laitting, P. Y. Cheng, K. F. Willey, and M. A. Duncan, Rev. Sci. Instrum. **63**, 2177 (1992).
[34] V. I. Karataev, B. A. Mamyrin, and D. V. Shmikk, Sov. Phys.-Tech. Phys. **16**, 1177 (1972).
[35] B. A. Mamyrin, V. I. Karataev, D. V. Shmikk, and V. A. Zagulin, Sov. Phys.-JETP **37**, 45 (1973).
[36] C. J. Thompson, J. Husband, F. Aguirre, and R. B. Metz, J. Phys. Chem. A **104**, 8155 (2000).
[37] K. P. Faherty, C. J. Thompson, F. Aguirre, J. Michne, and R. B. Metz, J. Phys. Chem. A **105**, 10054 (2001).
[38] C. J. Thompson, K. P. Faherty, K. L. Stringer, and R. B. Metz, J. Phys. Chem. A (to be submitted).
[39] L. N. Ding, P. D. Kleiber, M. A. Young, W. C. Stwalley, and A. M. Lyyra, Phys. Rev. A **48**, 2024 (1993).
[40] K. L. Stringer and R. B. Metz (in preparation).
[41] J. W. Buchanan, J. E. Reddic, G. A. Grieves, and M. A. Duncan, J. Phys. Chem. A **102**, 6390 (1998).
[42] K. M. Ervin, Chem. Rev. **101**, 391 (2001).
[43] P. B. Armentrout, Int. J. Mass Spectrom. **227**, 289 (2003).
[44] L. M. Russon, S. A. Heidecke, M. K. Birke, J. Conceicao, M. D. Morse, and P. B. Armentrout, J. Chem. Phys. **100**, 4747 (1994).
[45] J. Husband, F. Aguirre, C. J. Thompson, and R. B. Metz, Chem. Phys. Lett. **342**, 75 (2001).
[46] D. Lessen and P. J. Brucat, J. Chem. Phys. **91**, 4522 (1989).
[47] D. Lessen, R. L. Asher, and P. Brucat, Int. J. Mass Spec. Ion. Proc. **102**, 331 (1990).
[48] R. L. Asher, D. Bellert, T. Buthelezi, and P. J. Brucat, Chem. Phys. Lett. **227**, 277 (1994).
[49] K. K. Irikura and J. L. Beauchamp, J. Phys. Chem. **95**, 8344 (1991).
[50] K. K. Irikura and W. A. Goddard III, J. Am. Chem. Soc. **116**, 8733 (1994).
[51] R. Anderson, H. Kölbel, and M. Ralek, *The Fischer–Tropsch Synthesis* (Academic Press, Orlando, FL, 1984).
[52] R. H. Schultz and P. B. Armentrout, Organometallics **11**, 828 (1992).
[53] C. Heinemann, R. H. Hertwig, R. Wesendrup, W. Koch, and H. Schwarz, J. Am. Chem. Soc. **117**, 495 (1995).
[54] J. Hrusák, S. Afr. J. Chem. **50**, 93 (1997).

[55] F. Aguirre, J. Husband, C. J. Thompson, and R. B. Metz, Chem. Phys. Lett. **318**, 466 (2000).
[56] Production of CH_2 (a, $^1A_1$) at threshold would require $D_0 \leq 339\,kJ\,mol^{-1}$, which is significantly lower than the available experimental and theoretical data.
[57] A. K. Chowdhury and C. L. Wilkins, J. Am. Chem. Soc. **109**, 5336 (1987).
[58] J. R. Brown, P. Schwerdtfeger, D. Schröder, and H. Schwarz, J. Am. Soc. Mass Spectrom. **13**, 485 (2002).
[59] W. S. Taylor, J. C. May, and A. S. Lasater, J. Phys. Chem. A **107**, 2209 (2003).
[60] P. B. Armentrout and B. L. Kickel, in *Organometallic Ion Chemistry*, edited by B. S. Freiser (Kluwer Academic Publishers, Dordrecht, 1994).
[61] N. Sändig and W. Koch, Organometallics **16**, 5244 (1997).
[62] R. L. Hettich and B. S. Freiser, J. Am. Chem. Soc. **109**, 3543 (1987).
[63] A. Simon, J. Lemaire, P. Boissel, and P. Maitre, J. Chem. Phys. **115**, 2510 (2001).
[64] X. G. Zhang, R. Liyanage, and P. B. Armentrout, J. Am. Chem. Soc. **123**, 5563 (2001).
[65] U. Achatz, M. Beyer, S. Joos, B. S. Fox, G. Niedner-Schatteburg, and V. E. Bondybey, J. Phys. Chem. A **103**, 8200 (1999).
[66] T. Hayes, D. Bellert, T. Buthelezi, and P. J. Brucat, Chem. Phys. Lett. **264**, 220 (1997).
[67] J. Haggin, Chem. Eng. News **71**, 27 (1993).
[68] R. H. Crabtree, Chem. Rev. **95**, 987 (1995).
[69] B. K. Warren and S. T. Oyama, *Heterogeneous Hydrocarbon Oxidation* (American Chemical Society, Washington, DC, 1996).
[70] Y. Wang and K. Otsuka, J. Chem. Soc., Chem. Commun. **1994**, 2209 (1994).
[71] Y. Wang, K. Otsuka, and K. Ebitani, Catal. Lett. **35**, 259 (1995).
[72] H. Matsumoto, S. Tanabe, K. Okitsu, Y. Hayashi, and S. L. Suib, J. Phys. Chem. A **105**, 5304 (2001).
[73] R. A. Periana, D. J. Taube, S. Gamble, H. Taube, T. Satoh, and H. Fujii, Science **280**, 560 (1998).
[74] R. Raja and P. Ratnasamy, Appl. Catal. A **158**, L7 (1997).
[75] J. Haggin, Chem. Eng. News **72**, 24 (1994).
[76] A. C. Rosenzweig, C. A. Frederick, S. J. Lippard, and P. Nordlund, Nature **366**, 537 (1993).
[77] L. J. Shu, J. C. Nesheim, K. Kauffmann, E. Munck, J. D. Lipscomb, and L. Que, Science **275**, 515 (1997).
[78] D. Schröder and H. Schwarz, Angew. Chem., Intl. Ed. Engl. **29**, 1433 (1990).
[79] D. Schröder, H. Schwarz, D. E. Clemmer, Y. Chen, P. B. Armentrout, V. Baranov, and D. K. Bohme, Int. J. Mass Spectrom. Ion Proc. **161**, 175 (1997).
[80] Y.-M. Chen, D. E. Clemmer, and P. B. Armentrout, J. Am. Chem. Soc. **116**, 7815 (1994).
[81] A. Fiedler, D. Schröder, S. Shaik, and H. Schwarz, J. Am. Chem. Soc. **116**, 10734 (1994).
[82] K. Yoshizawa, Y. Shiota, and T. Yamabe, Chem. Eur. J. **3**, 1160 (1997).
[83] K. Yoshizawa, Y. Shiota, and T. Yamabe, J. Chem. Phys. **111**, 538 (1999).
[84] K. Yoshizawa, Y. Shiota, and T. Yamabe, J. Am. Chem. Soc. **120**, 564 (1998).
[85] Y. Shiota and K. Yoshizawa, J. Am. Chem. Soc. **122**, 12317 (2000).
[86] Y. Shiota and K. Yoshizawa, J. Chem. Phys. **118**, 5872 (2003).
[87] F. Aguirre, J. Husband, C. J. Thompson, K. L. Stringer, and R. B. Metz, J. Chem. Phys. **119**, 10194 (2003).
[88] R. B. Metz, in *Research Advances in Physical Chemistry*, edited by R. M. Mohan (Global, Trivandrum, 2001).
[89] H. Y. Afeefy, J. F. Liebman, and S. E. Stein, in *NIST Chemistry WebBook, NIST Standard Reference Database Number 69*, edited by W. G. Mallard and P. J. Linstrom (National Institute of Standards and Technology, Gaithersburg, MD, 2001).
[90] X. G. Zhang and P. B. Armentrout, J. Phys. Chem. A **107**, 8904 (2003).
[91] H. Schwarz and D. Schröder, Pure Appl. Chem. **72**, 2319 (2000).
[92] F. Aguirre, PhD Thesis, University of Massachusetts, 2002.
[93] D. Schröder, A. Fiedler, M. F. Ryan, and H. Schwarz, J. Phys. Chem. **98**, 68 (1994).
[94] M. Filatov and S. Shaik, J. Phys. Chem. A **102**, 3835 (1998).
[95] D. Danovich and S. Shaik, J. Am. Chem. Soc. **119**, 1773 (1997).

[96] D. Schröder, S. Shaik, and H. Schwarz, Acc. Chem. Res. **33**, 139 (2000).
[97] J. M. Dyke, B. W. J. Gravenor, M. P. Hastings, and A. Morris, J. Phys. Chem. **89**, 4613 (1985).
[98] J. M. Dyke, B. W. J. Gravenor, R. A. Lewis, and A. Morris, J. Chem. Soc., Faraday Trans. 1 **79**, 1083 (1983).
[99] J. M. Dyke, A. M. Ellis, M. Feher, A. Morris, A. J. Paul, and J. C. H. Stevens, J. Chem. Soc., Faraday Trans. II **83**, 1555 (1987).
[100] A. D. Sappey, G. Eiden, J. E. Harrington, and J. C. Weisshaar, J. Chem. Phys. **90**, 1415 (1989).
[101] J. Harrington and J. C. Weisshaar, J. Chem. Phys. **97**, 2809 (1992).
[102] J. F. Harrison, Chem. Rev. **100**, 679 (2000).
[103] E. A. Carter and W. A. Goddard III, J. Phys. Chem. **92**, 2109 (1988).
[104] M. Sodupe, V. Branchadell, M. Rosi, and C. W. Bauschlicher Jr, J. Phys. Chem. A **101**, 7854 (1997).
[105] Y. Nakao, K. Hirao, and T. Taketsugu, J. Chem. Phys. **114**, 7935 (2001).
[106] A. Fiedler, J. Hrusák, W. Koch, and H. Schwarz, Chem. Phys. Lett. **211**, 242 (1993).
[107] C. Heinemann, W. Koch, and H. Schwarz, Chem. Phys. Lett. **245**, 509 (1995).
[108] T. Borowski and E. Broclawik, Chem. Phys. Lett. **339**, 433 (2001).
[109] R. Wesendrup, D. Schröder, and H. Schwarz, Angew. Chem., Int. Ed. Engl. **33**, 1174 (1994).
[110] M. Pavlov, M. R. A. Blomberg, P. E. M. Siegbahn, R. Wesendrup, C. Heinemann, and H. Schwarz, J. Phys. Chem. A **101**, 1567 (1997).
[111] C. Heinemann, R. Wesendrup, and H. Schwarz, Chem. Phys. Lett. **239**, 75 (1995).
[112] F. Rakowitz, C. M. Marian, and B. Schimmelpfennig, Phys. Chem. Chem. Phys. **2**, 2481 (2000).
[113] A. Simon, L. MacAleese, P. Boissel, and P. Maitre, Int. J. Mass Spectrom. **219**, 457 (2002).
[114] D. Schröder, H. Schwarz, J. Hrusák, and P. Pyykkö, Inorg. Chem. **37**, 624 (1998).
[115] D. Schröder, M. Diefenbach, H. Schwarz, A. Schier, and H. Schmidbaur, in *Relativistic Effects in Heavy-Element Chemistry and Physics*, edited by B. A. Hess (John Wiley & Sons, New York, 2003).
[116] R. H. Hertwig, W. Koch, D. Schröder, H. Schwarz, J. Hrusák, and P. Schwerdtfeger, J. Phys. Chem. **100**, 12253 (1996).
[117] K. L. Stringer, M. Citir, and R. B. Metz (in preparation).
[118] C. J. Cassady and B. S. Freiser, J. Am. Chem. Soc. **106**, 6176 (1984).
[119] Y. A. Ranasinghe, T. J. MacMahon, and B. S. Freiser, J. Am. Chem. Soc. **114**, 9112 (1992).
[120] W.-Y. Lu, P. D. Kleiber, M. A. Young, and K.-H. Yang, J. Chem. Phys. **115**, 5823 (2001).
[121] W. Y. Lu, T. H. Wong, and P. D. Kleiber, Chem. Phys. Lett. **347**, 183 (2001).
[122] W. Y. Lu, T. H. Wong, Y. Sheng, A. T. Lytle, and P. D. Kleiber, J. Phys. Chem. A **107**, 984 (2003).
[123] A. Ranasinghe and B. S. Freiser, Chem. Phys. Lett. **200**, 135 (1992).
[124] D. R. A. Ranatunga and B. S. Freiser, Chem. Phys. Lett. **233**, 319 (1995).
[125] R. S. Walters, T. D. Jaeger, and M. A. Duncan, J. Phys. Chem. A **106**, 10482 (2002).
[126] R. Houriet, L. F. Halle, and J. L. Beauchamp, Organometallics **2**, 1818 (1983).
[127] R. Tonkyn, M. Ronan, and J. C. Weisshaar, J. Phys. Chem. **92**, 92 (1988).
[128] R. Georgiadis, E. R. Fisher, and P. B. Armentrout, J. Am. Chem. Soc. **111**, 4251 (1989).
[129] C. L. Haynes, E. R. Fisher, and P. B. Armentrout, J. Phys. Chem. **100**, 18300 (1996).
[130] P. A. M. van Koppen, M. T. Bowers, E. R. Fisher, and P. B. Armentrout, J. Am. Chem. Soc. **116**, 3780 (1994).
[131] R. J. Noll, S. S. Yi, and J. C. Weisshaar, J. Phys. Chem. A **102**, 386 (1998).
[132] E. L. Reichert and J. C. Weisshaar, J. Phys. Chem. A **106**, 5563 (2002).
[133] P. A. M. van Koppen, J. Brodbelt-Lustig, M. T. Bowers, D. V. Dearden, J. L. Beauchamp, E. R. Fisher, and P. B. Armentrout, J. Am. Chem. Soc. **113**, 2359 (1991).

[134] R. L. Hettich and B. S. Freiser, in *Fourier Transform Mass Spectrometry: Evolution, Innovation, and Applications*, edited by M. V. Buchanan (American Chemical Society, Washington, DC, 1987).
[135] K. F. Willey, P. Y. Cheng, M. B. Bishop, and M. A. Duncan, J. Am. Chem. Soc. **113**, 4721 (1991).
[136] Y. Q. Huang, Y. D. Hill, M. Sodupe, C. W. Bauschlicher, and B. S. Freiser, Inorg. Chem. **30**, 3822 (1991).
[137] H. F. Lee, F. W. Lin, and C. S. Yeh, J. Mass Spectrom. **36**, 493 (2001).
[138] Y.-S. Yang, W.-Y. Hsu, H.-F. Lee, Y.-C. Huang, C.-S. Yeh, and C.-H. Hu, J. Phys. Chem. A **103**, 11287 (1999).
[139] V. K. Nanayakkara and B. S. Freiser, J. Mass Spectrom. **32**, 475 (1997).
[140] Y. Q. Huang and B. S. Freiser, J. Am. Chem. Soc. **111**, 2387 (1989).
[141] Y. Q. Huang and B. S. Freiser, J. Am. Chem. Soc. **112**, 5085 (1990).
[142] Y. C. Xu, E. Garcia, B. S. Freiser, and C. W. Bauschlicher, Int. J. Mass Spectrom. Ion Proc. **158**, 249 (1996).
[143] R. C. Dunbar, in *Gas Phase Inorganic Chemistry*, edited by D. H. Russell (Plenum Press, New York, 1989).
[144] M. A. Hanratty, C. M. Paulsen, and J. L. Beauchamp, J. Am. Chem. Soc. **107**, 5074 (1985).
[145] P. I. Surya, D. R. A. Ranatunga, and B. S. Freiser, J. Am. Chem. Soc. **119**, 3351 (1997).
[146] P. I. Surya, L. M. Roth, D. R. A. Ranatunga, and B. S. Freiser, J. Am. Chem. Soc. **118**, 1118 (1996).
[147] P. Maitre, S. Le Caer, A. Simon, W. Jones, J. Lemaire, H. N. Mestdagh, M. Heninger, G. Mauclaire, P. Boissel, R. Prazeres, F. Glotin, and J. M. Ortega, Nucl. Instrum. Methods A **507**, 541 (2003).
[148] S. S. Brown, H. L. Berghout, and F. F. Crim, J. Chem. Phys. **105**, 8103 (1996).
[149] M. R. Furlanetto, N. L. Pivonka, T. Lenzer, and D. M. Neumark, Chem. Phys. Lett. **326**, 439 (2000).
[150] M. Okumura, L. I. Yeh, J. D. Meyers, and Y. T. Lee, J. Chem. Phys. **85**, 2328 (1986).
[151] P. Ayotte, C. G. Bailey, J. Kim, and M. A. Johnson, J. Chem. Phys. **108**, 444 (1998).
[152] F. F. Crim, Annu. Rev. Phys. Chem. **44**, 397 (1993).
[153] M. R. Sievers, Y. M. Chen, C. L. Haynes, and P. B. Armentrout, Int. J. Mass Spectrom. **196**, 149 (2000).